

Diffraction by a right-angled no-contrast penetrable wedge: recovery of far-field asymptotics

Valentin D. Kunz* and Raphael C. Assier†

Corresponding author: v_kunz@startmail.com

Abstract

We provide a description of the far-field encountered in the diffraction problem resulting from the interaction of a monochromatic plane-wave and a right-angled no-contrast penetrable wedge. To achieve this, we employ a two-complex-variable framework and use the analytical continuation formulae derived in (Kunz & Assier, QJMAM, 76(2), 2023) to recover the wave-field's geometrical optics components, as well as the cylindrical and lateral diffracted waves. We prove that the corresponding cylindrical and lateral diffraction coefficients can be expressed in terms of certain two-complex-variable spectral functions, evaluated at some given points.

1 Introduction

The present paper is a direct follow-up to (Kunz and Assier, 2023), wherein a two-complex-variable approach was employed in order to study the right-angled no-contrast penetrable wedge diffraction problem. This is a notoriously difficult problem, with two different wavenumbers inside and outside the wedge. So far, almost all of the methods that proved successful in the context of diffraction by a perfect wedge seem to fail in solving the penetrable wedge diffraction problem and thus, new methods need to be developed. As one of the building blocks of Keller's geometrical theory of diffraction (GTD) (Keller, 1962; Borovikov and Kinber, 1993), availability of such solution or far-field expansion would have a profound impact on diffraction theory overall. For such far-field expansion to be available, it is imperative to obtain analytical expressions of the corresponding diffraction coefficients, which are describing the amplitude of the diffracted far-field.

Although analytical expressions for the diffraction coefficients describing the cylindrical wave-fields emanating from the penetrable wedge's corner remain to be found, there are several methods to (approximately) compute them within some given regions. We refer to the introductions of (Kunz and Assier, 2022, 2023), as well as Chapter 4 of (Nethercote, 2019) for a (non-exhaustive) overview of the work done on the penetrable wedge diffraction problem.

The paper (Kunz and Assier, 2023) is part of an ongoing effort to apply multidimensional complex analysis to wave-diffraction problems, and other work in this direction includes (Assier and Shanin, 2019, 2021a,b; Assier and Abrahams, 2020, 2021; Kunz and Assier, 2022) and (Assier et al., 2022). Akin to what is done in the one-complex-variable Wiener-Hopf technique (Noble, 1958; Lawrie and Abrahams, 2007), whose key aspects are outlined in Fig. 1 (left), in (Kunz and Assier, 2023) it was shown that the right-angled no-contrast penetrable wedge diffraction problem admits a reformulation as a functional problem in \mathbb{C}^2 . This functional problem involves two unknown spectral functions Ψ_{++} and $\Phi_{3/4}$ in terms of which the physical fields ψ and ϕ_{sc}

*The University of Manchester, Department of Mathematics, Oxford Road, Manchester, M13 9PL, UK; University of Bologna, Department of Mathematics, Piazza di Porta S. Donato, 5, 40126 Bologna, Italy

†The University of Manchester, Department of Mathematics, Oxford Road, Manchester, M13 9PL, UK

(describing the scattered wave-fields on the interior and exterior of the wedge, respectively) can be expressed as the following inverse double Fourier-integrals.

$$\psi(\mathbf{x}) = \frac{1}{4\pi^2} \iint_{\mathbb{R}^2} \Psi_{++}(\boldsymbol{\alpha}) e^{-i\mathbf{x}\cdot\boldsymbol{\alpha}} d\boldsymbol{\alpha} \text{ and } \phi_{\text{sc}}(\mathbf{x}) = \frac{1}{4\pi^2} \iint_{\mathbb{R}^2} \Phi_{3/4}(\boldsymbol{\alpha}) e^{-i\mathbf{x}\cdot\boldsymbol{\alpha}} d\boldsymbol{\alpha}. \quad (1.1)$$

Here, we have introduced the notation $\mathbf{x} = (x_1, x_2) \in \mathbb{R}^2$ and $\boldsymbol{\alpha} = (\alpha_1, \alpha_2) \in \mathbb{C}^2$, which will be used throughout the article. Moreover, following the work of Assier and Shanin (2019), the analyticity properties of Ψ_{++} and $\Phi_{3/4}$ were studied in (Kunz and Assier, 2023), and their singularity structure within \mathbb{C}^2 was unveiled. Although the results obtained in (Kunz and Assier, 2023) do

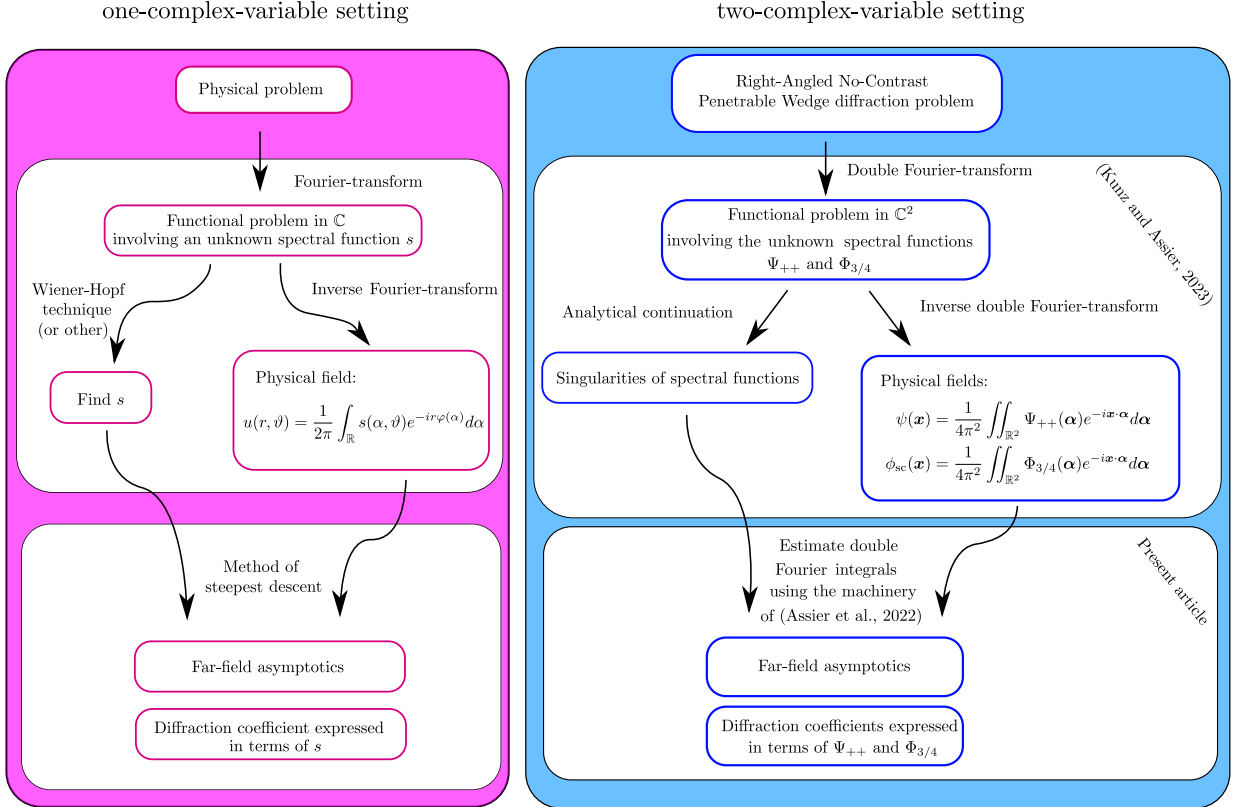


Figure 1: Diagrammatic comparison of obtaining far-field asymptotics in the context of the classical, one-complex-variable, setting and the two-complex-variable setting whereon the present article is based.

not yet allow one to complete the two-complex-variable Wiener-Hopf technique, knowledge of the spectral functions' singularities allows for obtaining closed-form far-field asymptotics of the physical wave-fields, which are described by (1.1) and obtaining such far-field asymptotics is the principal goal of the present article. The machinery required to achieve this was recently developed by Assier, Shanin, and Korolkov in (Assier et al., 2022) and used to recover the far-field asymptotics of the three-dimensional quarter plane problem in (Assier et al., 2023). Particularly, in the present article we will show that, akin to the classical one-complex-variable Wiener-Hopf setting, the diffraction coefficients describing the cylindrical corner diffracted waves, as well as the diffraction coefficients describing the so-called *lateral* diffracted waves, can be expressed in terms of the two-complex-variable spectral functions, evaluated at some given points. These aspects are illustrated in Fig. 1, right.

The content of the present article is organised as follows. After formulating the physical diffraction problem in Section 2 and introducing some notation in Section 3, we give an informal description of its far-field in Section 4 by using Keller's GTD. This article's main goal is to

rigorously prove the correctness of such far-field expansion. In Section 5, the theoretical framework required to achieve this is provided, and throughout Sections 6 and 7, closed-form far-field asymptotics of ψ and ϕ_{sc} which are in agreement with Keller’s GTD are derived. We show that both the cylindrical and lateral diffraction coefficients can be expressed in terms of the spectral functions Ψ_{++} and $\Phi_{3/4}$, evaluated at some given points. Another aim of this article is related to Sommerfeld’s radiation condition. In the context of diffraction by wedges, Sommerfeld’s radiation condition relies on a-priori knowledge of the physical wave-field’s geometrical optics (GO) components, which, in some sense, serve as some additional boundary conditions as was pointed out by [Stoker \(1956\)](#). In Section 7, we give a formulation of the radiation which does not require a-priori knowledge of these components.

2 Problem formulation

Consider a plane-wave ϕ_{in} incident on an infinite, right-angled, penetrable wedge (PW) given by

$$\text{PW} = \{(x_1, x_2) \in \mathbb{R}^2 \mid x_1 \geq 0, x_2 \geq 0\},$$

as illustrated in Fig. 2 (left).

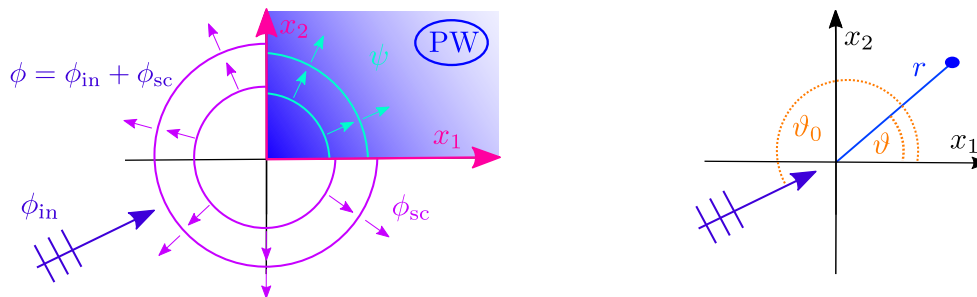


Figure 2: Left: Illustration of the problem described by equations (2.1)–(2.4), taken from ([Kunz and Assier, 2023](#)). Right: Polar coordinate system and incident angle ϑ_0 of ϕ_{in} .

We assume transparency of the wedge and thus expect a scattered field ϕ_{sc} in $\mathbb{R}^2 \setminus \text{PW}$ and a transmitted field ψ in PW. Moreover, we assume time-harmonic with the $e^{-i\omega t}$ convention, and the time-dependence is henceforth suppressed. Therefore, the wave-fields’ dynamics are described by two Helmholtz equations, and the incident wave (only supported within $\mathbb{R}^2 \setminus \text{PW}$) is given by

$$\phi_{\text{in}}(\mathbf{x}) = e^{i\mathbf{k}_1 \cdot \mathbf{x}}$$

where $\mathbf{k}_1 \in \mathbb{R}^2$ is the incident wave vector and $\mathbf{x} = (x_1, x_2) \in \mathbb{R}^2$. Additionally, we are describing a *no-contrast penetrable wedge*, meaning that the *contrast parameter* λ satisfies

$$\lambda = 1.$$

This contrast parameter corresponds to either the ratio of magnetic permittivities or electric permeabilities, in the electromagnetic setting, or to the ratio of densities, in the acoustic setting. We refer to ([Kunz and Assier, 2022, 2023](#)) for a more detailed description of the physical context.

Let $k_1 = |\mathbf{k}_1| = \omega/c_1$ and $k_2 = \omega/c_2$ denote the wavenumbers inside and outside PW, respectively, where c_1 and c_2 are the wave speeds relative to the media in $\mathbb{R}^2 \setminus \text{PW}$ and PW, respectively. Note that, although $\lambda = 1$, we assume that $c_1 \neq c_2$, and so $k_1 \neq k_2$. Setting $\phi = \phi_{\text{sc}} + \phi_{\text{in}}$ (the total wave-field in $\mathbb{R}^2 \setminus \text{PW}$), and letting \mathbf{n} denote the inward pointing normal on ∂PW , the diffraction problem at hand is then described by the following equations.

$$\Delta\phi + k_1^2\phi = 0 \quad \text{in } \mathbb{R}^2 \setminus \text{PW}, \quad (2.1)$$

$$\Delta\psi + k_2^2\psi = 0 \quad \text{in PW}, \quad (2.2)$$

$$\phi = \psi \quad \text{on } \partial\text{PW}, \quad (2.3)$$

$$\partial_n\phi = \partial_n\psi \quad \text{on } \partial\text{PW}. \quad (2.4)$$

In the electromagnetic setting, ϕ and ψ correspond either to the electric or magnetic field (depending on the polarization of the incident wave, cf. (Radlow, 1964; Kraut and Lehmann, 1969)) in $\mathbb{R}^2 \setminus \text{PW}$ and PW , respectively, whereas in the acoustic setting, ϕ and ψ represent the total pressure in $\mathbb{R}^2 \setminus \text{PW}$ and PW , respectively.

Introducing polar coordinates (r, ϑ) , we rewrite the incident wave vector as $\mathbf{k}_1 = -k_1(\cos(\vartheta_0), \sin(\vartheta_0))$ where ϑ_0 is the incident angle as shown on Fig. 2, right. We rewrite the incident wave as

$$\phi_{\text{in}} = e^{-i(\mathbf{a}_1 x_1 + \mathbf{a}_2 x_2)} \quad (2.5)$$

with

$$\mathbf{a}_1 = k_1 \cos(\vartheta_0) \text{ and } \mathbf{a}_2 = k_1 \sin(\vartheta_0). \quad (2.6)$$

For the problem to be well posed, and uniquely solvable, we also require the fields to satisfy the Sommerfeld radiation condition, meaning that the wave-field should be outgoing in the far-field, and edge conditions called ‘Meixner conditions’, ensuring finiteness of the wave-field’s energy near the tip (see (Babich and Mokeeva, 2008)). The edge conditions are given by

$$\phi(r, \vartheta) = B + (A_1 \sin(\vartheta) + B_1 \cos(\vartheta))r + \mathcal{O}(r^2) \text{ as } r \rightarrow 0, \quad (2.7)$$

$$\psi(r, \vartheta) = B + (A_1 \sin(\vartheta) + B_1 \cos(\vartheta))r + \mathcal{O}(r^2) \text{ as } r \rightarrow 0. \quad (2.8)$$

Note that (2.7) and (2.8) are only valid when $\lambda = 1$, and we refer to (Nethercote et al., 2020) for the general case.

To formulate the radiation condition, we henceforth consider two different cases, coined the ‘simple case’ and the ‘complicated case’, respectively. In these respective cases, different types of GO components are present as illustrated in Fig. 4. The simple case corresponds to $\vartheta_0 \in (\pi, 3\pi/2)$, which ensures that, for positive imaginary part $\varkappa = \text{Im}(k_1) = \text{Im}(k_2) > 0$ of the wavenumbers, we have $\text{Im}(\mathbf{a}_1) < 0$ and $\text{Im}(\mathbf{a}_2) < 0$. In this case, the formulation of the radiation condition is straightforward: For $\varkappa > 0$, the scattered and transmitted fields, ϕ_{sc} and ψ , decay exponentially as $r \rightarrow \infty$. In the complicated case, when $\vartheta_0 \in (\pi/2, \pi)$ or $\vartheta_0 \in (3\pi/2, 2\pi)$, formulating the radiation condition on the scattered and transmitted fields is not so straightforward, and will be discussed in detail in Section 7.

Throughout this article, we assume that $\vartheta_0 \neq \pi$ and that $\vartheta_0 \neq 3\pi/2$ (i.e. we do not consider the case of grazing incidence), and we assume that $\vartheta_0 \notin (0, \pi/2)$ (i.e. the wave is incident *on* the wedge). The reason for these assumptions will be explained in Sections 6 and 7. Moreover, due to the symmetry of the wedge, we assume without loss of generality that $\vartheta_0 \in (\pi/2, 5\pi/4]$.

3 An important function

Before we proceed, let us introduce the function $\sqrt[\vee]{\alpha}$, which will be extensively used throughout the remainder of this article. We define it as the square root with branch cut on the positive real axis, and with branch determined by $\sqrt[\vee]{1} = 1$ (i.e. $\arg(\alpha) \in [0, 2\pi)$). In particular, $\text{Im}(\sqrt[\vee]{\alpha}) \geq 0$ for all α and $\text{Im}(\sqrt[\vee]{\alpha}) = 0$ if, and only if, $\alpha \in (0, \infty)$. For fixed k_j (where $j = 1, 2$), the function

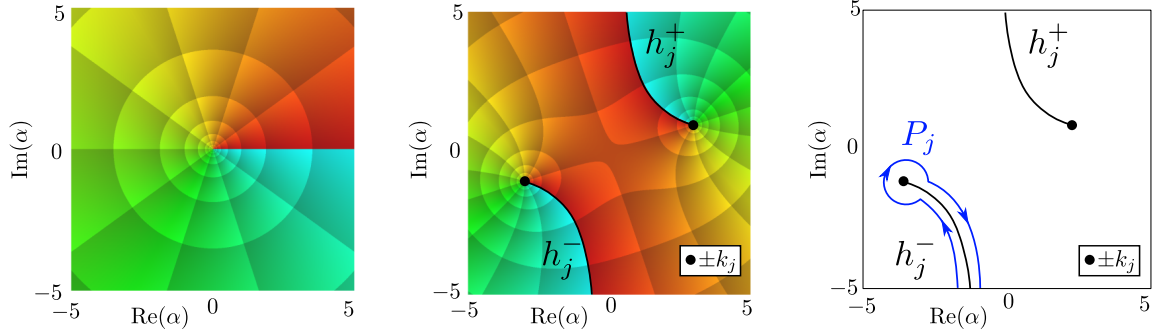


Figure 3: Phase portraits of the functions $\sqrt{\alpha}$ (left) and $\sqrt{k_j^2 - \alpha^2}$ ($j = 1$ or $j = 2$) for $k_j = 3 + i$ (centre), illustration of the branch cuts h^+ and h^- (centre and right), and of the contour P_j (right).

$\sqrt{k_j^2 - \alpha^2}$ has two branch points, at $\alpha = +k_j$ and $\alpha = -k_j$, respectively, and two corresponding branch cuts h_j^+ and h_j^- , which are given by

$$h_j^+ = \left\{ \sqrt{k_j^2 - x^2} \mid x \in \mathbb{R} \right\} \quad \text{and} \quad h_j^- = \left\{ -\sqrt{k_j^2 - x^2} \mid x \in \mathbb{R} \right\}. \quad (3.1)$$

The functions $\sqrt{\alpha}$, $\sqrt{k_j^2 - \alpha^2}$, and the branch cuts h_j^+ and h_j^- are visualised in Fig. 3. Moreover, let us define the contour P_j as the (oriented) boundary of $\mathbb{C} \setminus h_j^-$, see Fig. 3. That is, for $j = 1, 2$, P_j is the contour ‘starting at $-i\infty$ ’ and moving up along h_j^- ’s left side, up to $-k_j$, and then moving back towards $-i\infty$ along h_j^- ’s right side. Intuitively, P_j is just h_j^- but ‘keeps track’ of which side h_j^- was approached from. We set $P = P_1 \cup P_2$ (this contour will be used throughout Sections 5–7).

Notation. Whenever $\alpha \in (0, \infty)$, we write $\sqrt{\alpha} = \sqrt{\alpha}$ for simplicity. This is because for such α , the function $\sqrt{\alpha}$ agrees with the usual square root function on the positive real numbers.

4 Informal description of the far-field

As $r = |\mathbf{x}| \rightarrow \infty$, according to Keller’s GTD (Keller, 1962), we expect that the wave-fields can be described by their GO components (ϕ_{GO} and ψ_{GO} , respectively), as well as the corresponding diffracted wave-fields resulting from the interaction of ϕ_{in} with the wedge’s corner. In the far-field, the diffracted field splits into cylindrical and lateral diffracted waves, which we denote by ϕ_{C} , ψ_{C} , and ϕ_{L_1} , ϕ_{L_2} , ψ_{L_1} , ψ_{L_2} , respectively. Therefore, overall, we should obtain

$$\phi \sim \phi_{\text{GO}} + \phi_{\text{C}} + \phi_{\text{L}_1} + \phi_{\text{L}_2}, \quad \text{and} \quad \psi \sim \psi_{\text{GO}} + \psi_{\text{C}} + \psi_{\text{L}_1} + \psi_{\text{L}_2}, \quad \text{as } r \rightarrow \infty, \quad (4.1)$$

This article’s main endeavour is to prove the correctness of (4.1) and obtain formulae for the wave components ϕ_{GO} , ϕ_{C} , ϕ_{L_1} , ϕ_{L_2} , ψ_{GO} , ψ_{C} , ψ_{L_1} , and ψ_{L_2} . This will be the subject of Sections 6 (simple case) and 7 (complicated case), respectively.

The fields’ GO components are well understood and explicit formulae for ϕ_{GO} and ψ_{GO} will be provided throughout Sections 6 and 7. The fields’ GO components are displayed in Fig. 4 left (simple case) and right (complicated case).

The cylindrical diffracted waves ϕ_{C} and ψ_{C} are a well known type of wave as well. Although no analytical description is available for them, many ways to efficiently compute them have been found. We refer to the introduction of (Kunz and Assier, 2023) for an overview of the work done on computing the diffracted far-field. However, the cylindrical diffracted waves are discontinuous

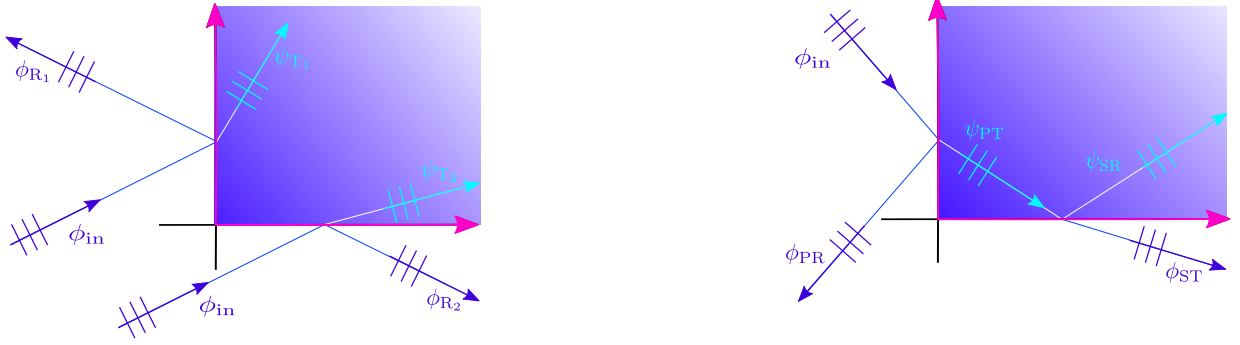


Figure 4: Geometrical optics components of the wave-fields ϕ and ψ in the simple case (left) and in the complicated case (right). The subscripts $R_j, T_j, j = 1,2$ correspond to the two reflected and transmitted plane waves, whereas the subscripts $PR, PT, SR,$ and ST correspond to ‘primary reflected’, ‘primary transmitted’, ‘secondary reflected’, and ‘secondary transmitted’, respectively.

across the wedges interface so some additional ‘lateral waves’ are required to ensure continuity of the total wave-fields. These diffracted lateral waves $\phi_{L1}, \phi_{L2}, \psi_{L1},$ and ψ_{L2} are not as well studied. Thus, we briefly introduce this type of wave in the following section.

4.1 Diffraction by a penetrable interface

Consider the two half-spaces $\Omega_1 = \{(x_1, x_2) \in \mathbb{R}^2 \mid x_1 > 0\}$ and $\Omega_2 = \{(x_1, x_2) \in \mathbb{R}^2 \mid x_1 < 0\}$. We will study the diffraction problem resulting from the point source incidence given by

$$\tilde{\phi}_{in}(\mathbf{x}) = -\frac{i}{4} H_0^{(1)}(k_1 |\mathbf{x} - \mathbf{x}_0|), \quad \mathbf{x}_0 \in \Omega_1. \quad (4.2)$$

Without loss of generality, we may assume that the point source is located along the x_2 -axis, and we can thus write $\mathbf{x}_0 = (0, b), b \geq 0$, cf. Fig. 5.

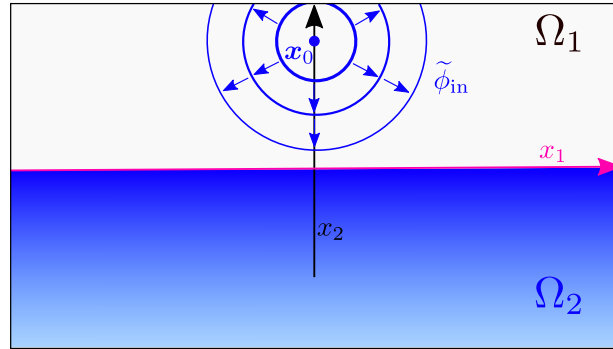


Figure 5: Cylindrical wave $\tilde{\phi}_{in}$ emanating from a point source at \mathbf{x}_0 in Ω_1 , which is incident on a half-space Ω_2 whose boundary is the x_1 -axis.

Akin to the penetrable wedge diffraction problem formulated in Section 2, let us denote the scattered field within Ω_1 by $\tilde{\phi}_{sc}$, and the total wave-field within Ω_2 by $\tilde{\psi}$. Denote the wavenumbers within Ω_1 and Ω_2 , respectively, by k_1 and k_2 . Then, the solution to the corresponding diffraction

problem subject to Sommerfeld's radiation condition is given by¹

$$\tilde{\phi}_{\text{sc}}(\mathbf{x}) = \frac{i}{4\pi} \int_{\mathbb{R}} \frac{\sqrt{k_1^2 - \alpha^2} - \sqrt{k_2^2 - \alpha^2}}{\sqrt{k_1^2 - \alpha^2} + \sqrt{k_2^2 - \alpha^2}} \frac{e^{i(-\alpha x_1 + \sqrt{k_1^2 - \alpha^2}(x_2 + b))}}{\sqrt{k_1^2 - \alpha^2}} d\alpha, \quad (4.3)$$

$$\tilde{\psi}(\mathbf{x}) = \frac{i}{4\pi} \int_{\mathbb{R}} \frac{2\sqrt{k_1^2 - \alpha^2}}{\sqrt{k_1^2 - \alpha^2} + \sqrt{k_2^2 - \alpha^2}} \frac{e^{i(-\alpha x_1 - \sqrt{k_2^2 - \alpha^2}x_2 + \sqrt{k_1^2 - \alpha^2}b)}}{\sqrt{k_1^2 - \alpha^2}} d\alpha. \quad (4.4)$$

These formulae are well-known and are given, for instance, in (Brekhovskikh and Godin, 1999). We refer to (Kunz, 2023), Section 1.3 for their detailed derivation.

Far-field asymptotics. The far-field asymptotics of $\tilde{\phi}_{\text{sc}}$ and $\tilde{\psi}$ can be obtained by means of the method of steepest descent. We will be brief, and refer to (Kunz, 2023), Section 1.3, and to the book of Brekhovskikh and Godin (1999) for a more detailed discussion. Let us assume that $\text{Im}(k_1) = \text{Im}(k_2) = 0$, and that $k_1 > 0$ as well as $k_2 > 0$. The integrals in (4.3) and (4.4) have a saddle point at $\alpha = -k_1 \cos(\vartheta)$ and $\alpha = -k_2 \cos(\vartheta)$, respectively. From these saddle points, we obtain a reflected and transmitted cylindrical wave which we call $\tilde{\phi}_{\text{C}}$ and $\tilde{\psi}_{\text{C}}$, respectively. However, depending on ϑ and whether $k_1 > k_2$ or $k_2 > k_1$, contributions of the branch points of the integrands need to be taken into account².

For $k_1 > k_2$, these yield the *lateral waves* within Ω_1 , whose leading order approximation we denote by $\tilde{\phi}_{\text{L}_1}$ and $\tilde{\phi}_{\text{L}_2}$, and for $k_2 > k_1$ these yield the lateral waves within Ω_2 , with corresponding leading order approximation denoted by $\tilde{\psi}_{\text{L}_1}$ and $\tilde{\psi}_{\text{L}_2}$. For $k_1 > k_2$, they are given by

$$\tilde{\phi}_{\text{L}_1}(r, \vartheta) = \frac{i}{2\sqrt{\pi}} \frac{\sqrt{2k_2}}{(k_1^2 - k_2^2)^{1/4}} e^{i3\pi/4} e^{i\sqrt{k_1^2 - k_2^2}b} \frac{e^{ir(\cos(\vartheta)k_2 + \sqrt{k_1^2 - k_2^2}\sin(\vartheta))}}{|\sqrt{k_1^2 - k_2^2}r \cos(\vartheta) - k_2 r \sin(\vartheta)|^{3/2}}, \quad (4.5)$$

for $\vartheta \in (0, \arccos(k_2/k_1))$ (and $\tilde{\phi}_{\text{L}_1} \equiv 0$ otherwise), and

$$\tilde{\phi}_{\text{L}_2}(r, \vartheta) = \frac{i}{2\sqrt{\pi}} \frac{\sqrt{2k_2}}{(k_1^2 - k_2^2)^{1/4}} e^{i3\pi/4} e^{i\sqrt{k_1^2 - k_2^2}b} \frac{e^{ir(-\cos(\vartheta)k_2 + \sqrt{k_1^2 - k_2^2}\sin(\vartheta))}}{|\sqrt{k_1^2 - k_2^2}r \cos(\vartheta) + k_2 r \sin(\vartheta)|^{3/2}}, \quad (4.6)$$

for $\vartheta \in (\pi - \arccos(k_2/k_1), \pi)$ (and $\tilde{\phi}_{\text{L}_2} \equiv 0$ otherwise).

For $k_2 > k_1$, they are given by

$$\tilde{\psi}_{\text{L}_1}(r, \vartheta) = \frac{i}{4\sqrt{\pi}} \frac{\sqrt{2k_1} e^{i3\pi/4}}{(k_2^2 - k_1^2)^{1/4}} \frac{e^{ir(\cos(\vartheta)k_1 - \sqrt{k_2^2 - k_1^2}\sin(\vartheta))}}{|\sqrt{k_2^2 - k_1^2}r \cos(\vartheta) + k_1 r \sin(\vartheta)|^{3/2}}, \quad (4.7)$$

and

$$\tilde{\psi}_{\text{L}_2}(r, \vartheta) = \frac{i}{4\sqrt{\pi}} \frac{\sqrt{2k_1} e^{i3\pi/4}}{(k_2^2 - k_1^2)^{1/4}} \frac{e^{ir(-\cos(\vartheta)k_1 - \sqrt{k_2^2 - k_1^2}\sin(\vartheta))}}{|-\sqrt{k_2^2 - k_1^2}r \cos(\vartheta) + k_1 r \sin(\vartheta)|^{3/2}}. \quad (4.8)$$

Although $\tilde{\psi}_{\text{L}_1}$ and $\tilde{\psi}_{\text{L}_2}$ are independent of b , the transmitted field's lateral waves do, in fact, depend on b , but this dependence only appears for higher order correction terms. Whenever

¹In the following formulae, the contour of integration is chosen to be \mathbb{R} . It is valid for $\text{Im}(k_{1,2}) > 0$, but for $\text{Im}(k_1) = \text{Im}(k_2) = 0$, it needs to be an indented contour avoiding the integrands' singularities. By imposing that the scattered fields decay exponentially for positive imaginary part of the wave-numbers, finding this indentation is straightforward. We omit the details and refer to (Brekhovskikh and Godin, 1999).

²The integrands' polar singularities pose no problem, as is explained in (Brekhovskikh and Godin, 1999).

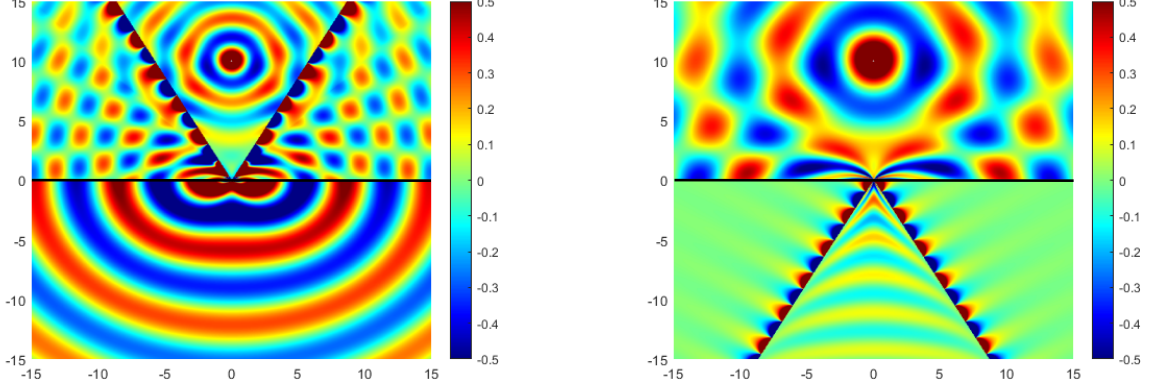


Figure 6: Plot of the wave-fields' far-field asymptotics for $k_1 = 2$ and $k_2 = 1$ (left), and $k_1 = 1$ and $k_2 = 2$ (right). Here, we have $b = 10$.

$\vartheta \notin (-\arccos(k_1/k_2), 0)$, we have $\tilde{\psi}_{L_1} \equiv 0$, and whenever $\vartheta \notin (-\pi, -\pi + \arccos(k_1/k_2))$, we have $\tilde{\psi}_{L_2} \equiv 0$. For $j = 1, 2$, let us set $\tilde{\phi}_{L_j} \equiv 0$ whenever $k_1 \leq k_2$ and $\tilde{\psi}_{L_j} \equiv 0$ whenever $k_2 \leq k_1$. Overall, as $r \rightarrow \infty$, we then obtain

$$\tilde{\phi}_{\text{sc}} \sim \tilde{\phi}_{\text{C}} + \tilde{\phi}_{L_1} + \tilde{\phi}_{L_2} \quad \text{and} \quad \tilde{\psi} \sim \tilde{\psi}_{\text{C}} + \tilde{\psi}_{L_1} + \tilde{\psi}_{L_2}, \quad (4.9)$$

where

$$\tilde{\phi}_{\text{C}}(r, \vartheta) = -\frac{i}{4} \frac{\sqrt{k_1^2 - k_1^2 \cos^2(\vartheta)} - \sqrt{k_2^2 - k_1^2 \cos^2(\vartheta)}}{\sqrt{k_1^2 - k_1^2 \cos^2(\vartheta)} + \sqrt{k_2^2 - k_1^2 \cos^2(\vartheta)}} e^{k_1 \sin(\vartheta)b} H_0^{(1)}(k_1 r), \quad (4.10)$$

and

$$\tilde{\psi}_{\text{C}}(r, \vartheta) = -\frac{i}{2} \frac{\sqrt{k_1^2 - k_2^2 \cos^2(\vartheta)}}{\sqrt{k_1^2 - k_2^2 \cos^2(\vartheta)} + \sqrt{k_2^2 - k_2^2 \cos^2(\vartheta)}} e^{i\sqrt{k_1^2 - k_2^2 \cos^2(\vartheta)}b} H_0^{(1)}(k_2 r). \quad (4.11)$$

The far-field asymptotics of $\tilde{\phi}$ and $\tilde{\psi}$ are shown in Fig. 6.

Notation. Henceforth, we shall also refer to the lateral waves' leading order approximation as 'the' lateral wave. That is, we refer to $\tilde{\phi}_{L_j}$ and $\tilde{\psi}_{L_j}$, $j = 1, 2$ as lateral waves, and similarly for the penetrable wedge diffraction problem. This is consistent with the notation used in (4.1). Since we will only be interested in such leading order approximations, this notation is unambiguous.

Note that the lateral waves $\tilde{\phi}_{L_1}$ and $\tilde{\phi}_{L_2}$ decay away from the lines $\vartheta \equiv \arccos(k_2/k_1)$ and $\vartheta \equiv \pi - \arccos(k_2/k_1)$, respectively, whereas the lateral waves $\tilde{\psi}_{L_1}$ and $\tilde{\psi}_{L_2}$ decay away from the lines $\vartheta \equiv -\arccos(k_1/k_2)$ and $\vartheta \equiv -\pi + \arccos(k_1/k_2)$, respectively. On these lines, the lateral waves are undefined, which is due to the coalescence of the respective branch points and the saddle point of the integrands in equations (4.3) and (4.4). So, on these lines, the diffracted wave does not split into cylindrical and lateral waves. Such coalescence also occurs for $\vartheta = 0$ or $\vartheta = \pi$, so, on the interface, the diffracted wave does not split as well. Finally, note that since the lateral waves are of order $\mathcal{O}(r^{-3/2})$, they decay faster than the corresponding cylindrical waves, which are of order $\mathcal{O}(r^{-1/2})$. For more on lateral waves, their physical meaning, and their relevance, we refer to (Brekhovskikh and Godin, 1999), Chapter 3.

5 Background and setup

To prove the correctness of (4.1), we will rely on using the frameworks recently developed in (Kunz and Assier, 2023) and (Assier et al., 2022). Thus, we summarise these papers' key results in Sections 5.1 and 5.2, respectively.

5.1 Summary of (Kunz and Assier, 2023)

As before, let

$$\varkappa = \text{Im}(k_{1,2}) \geq 0$$

denote the imaginary part of k_1 and k_2 . In the following formulae, we omit the argument \varkappa for brevity. Let $\boldsymbol{\alpha} = (\alpha_1, \alpha_2) \in \mathbb{C}^2$, set $\psi \equiv 0$ within $\mathbb{R}^2 \setminus \text{PW}$ and $\phi_{\text{sc}} \equiv 0$ within PW , and introduce the (unknown) spectral functions Ψ_{++} and $\Phi_{3/4}$ via

$$\Psi_{++}(\boldsymbol{\alpha}) = \iint_{\mathbb{R}^2} \psi(\mathbf{x}) e^{i\boldsymbol{\alpha} \cdot \mathbf{x}} d\mathbf{x}, \text{ and } \Phi_{3/4}(\boldsymbol{\alpha}) = \iint_{\mathbb{R}^2} \phi_{\text{sc}}(\mathbf{x}) e^{i\boldsymbol{\alpha} \cdot \mathbf{x}} d\mathbf{x}.$$

Then, according to Theorem 4.2.1 of (Kunz and Assier, 2023), these spectral functions satisfy the following two-complex-variable Wiener-Hopf functional equation

$$-K(\boldsymbol{\alpha})\Psi_{++}(\boldsymbol{\alpha}) = \Phi_{3/4}(\boldsymbol{\alpha}) + P_{++}(\boldsymbol{\alpha}), \quad (5.1)$$

where the kernel K and the forcing P_{++} are given by

$$K(\boldsymbol{\alpha}) = \frac{k_2^2 - \alpha_1^2 - \alpha_2^2}{k_1^2 - \alpha_1^2 - \alpha_2^2} \quad \text{and} \quad P_{++}(\boldsymbol{\alpha}) = \frac{1}{(\mathbf{a}_1 - \alpha_1)(\mathbf{a}_2 - \alpha_2)}. \quad (5.2)$$

The Wiener-Hopf equation is valid in the (common) domain of analyticity of K , P_{++} , Ψ_{++} , and $\Phi_{3/4}$, which includes some open neighbourhood $U \subset \mathbb{C}^2$ of \mathbb{R}^2 . We proceed to describe this analyticity structure. To this end, let us introduce the following sets.

$$\text{UHP} = \{\alpha \in \mathbb{C} \mid \text{Im}(\alpha) \geq 0\}, \text{ LHP} = \{\alpha \in \mathbb{C} \mid \text{Im}(\alpha) \leq 0\}, \text{ } H^- = \text{LHP} \setminus (h_1^- \cup h_2^-).$$

henceforth, when speaking of analyticity of a function on a closed set, it is implied that there is some open neighbourhood of the set's boundary whereon this function is analytic. Let

$$\mathcal{I}_1(\boldsymbol{\alpha}; z_1) = \frac{(k_2^2 - k_1^2) \Psi_{++} \left(z_1, \sqrt{k_1^2 - z_1^2} \right)}{K_{-o}(z_1, \alpha_2)(z_1 - \alpha_1) \left(\sqrt{k_1^2 - z_1^2} - \alpha_2 \right) \sqrt{k_1^2 - z_1^2}}, \quad (5.3)$$

$$\mathcal{I}_2(\boldsymbol{\alpha}; z_2) = \frac{(k_2^2 - k_1^2) \Psi_{++} \left(\sqrt{k_1^2 - z_2^2}, z_2 \right)}{K_{o-}(\alpha_1, z_2)(z_2 - \alpha_2) \left(\sqrt{k_1^2 - z_2^2} - \alpha_1 \right) \sqrt{k_1^2 - z_2^2}}. \quad (5.4)$$

Then, in the simple case, for $\varkappa > 0$, the following formulae for analytic continuation can be used to prove that the function $\Psi_{++}(\boldsymbol{\alpha})$ is analytic within the domain

$$\left(\text{UHP} \times \mathbb{C} \setminus (h_1^- \cup h_2^- \cup \{\mathbf{a}_2\}) \right) \cup \left(\mathbb{C} \setminus (h_1^- \cup h_2^- \cup \{\mathbf{a}_1\}) \times \text{UHP} \right).$$

$$\Psi_{++}(\boldsymbol{\alpha}) = \frac{-i}{4\pi K_{o+}(\boldsymbol{\alpha})} \int_P \mathcal{I}_2(\boldsymbol{\alpha}; z_2) dz_2 - \frac{K_{-o}(\alpha_1, \mathbf{a}_2) P_{++}(\boldsymbol{\alpha})}{K_{o+}(\boldsymbol{\alpha}) K_{o-}(\alpha_1, \mathbf{a}_2) K_{-o}(\mathbf{a}_1, \mathbf{a}_2)}, \quad (5.5)$$

$$\Psi_{++}(\boldsymbol{\alpha}) = \frac{-i}{4\pi K_{+o}(\boldsymbol{\alpha})} \int_P \mathcal{I}_1(\boldsymbol{\alpha}; z_1) dz_1 - \frac{K_{o-}(\mathbf{a}_1, \alpha_2) P_{++}(\boldsymbol{\alpha})}{K_{+o}(\boldsymbol{\alpha}) K_{-o}(\mathbf{a}_1, \alpha_2) K_{o-}(\mathbf{a}_1, \mathbf{a}_2)}, \quad (5.6)$$

where the contour P was defined in Section 3. Formula (5.5) is valid within the domain $H^- \setminus \{\mathbf{a}_1\} \times \text{UHP}$ whereas formula (5.6) is valid within $\text{UHP} \times H^- \setminus \{\mathbf{a}_2\}$. Upon multiplication by K , formulae (5.5) and (5.6) can be used to analytically continue $\Phi_{3/4}$ onto the domain $(H^- \setminus \{\mathbf{a}_1\}) \times (H^- \setminus \{\mathbf{a}_2\})$. Recall that we have $\mathbf{a}_1 = k_1 \cos(\vartheta_0)$ and $\mathbf{a}_2 = k_1 \sin(\vartheta_0)$, where ϑ_0 is the incident angle (cf. Section 2), and

$$K_{-\circ}(\boldsymbol{\alpha}) = \frac{\sqrt[k_2^2 - \alpha_2^2 - \alpha_1]{}}{\sqrt[k_1^2 - \alpha_2^2 - \alpha_1]{}}, \quad K_{+\circ}(\boldsymbol{\alpha}) = \frac{\sqrt[k_2^2 - \alpha_2^2 + \alpha_1]{}}{\sqrt[k_1^2 - \alpha_2^2 + \alpha_1]{}}, \quad (5.7)$$

$$K_{\circ-}(\boldsymbol{\alpha}) = \frac{\sqrt[k_2^2 - \alpha_1^2 - \alpha_2]{}}{\sqrt[k_1^2 - \alpha_1^2 - \alpha_2]{}}, \quad K_{\circ+}(\boldsymbol{\alpha}) = \frac{\sqrt[k_2^2 - \alpha_1^2 + \alpha_2]{}}{\sqrt[k_1^2 - \alpha_1^2 + \alpha_2]{}}, \quad (5.8)$$

where the function $\sqrt[\alpha]{}$ is as defined in Section 3, and we have $K = K_{\circ+}K_{\circ-} = K_{+\circ}K_{-\circ}$.

In (Kunz and Assier, 2023), it was proved that from the spectral functions, the physical fields ψ and ϕ can be obtained via (1.1).

As already mentioned, formulae (5.5)–(5.6) have been derived for the simple case $\vartheta_0 \in (\pi, 3\pi/2)$ and for $\varkappa > 0$ only. However, these formulae remain valid in the limit $\varkappa \rightarrow 0$, provided that the integration contours are appropriately changed to avoid the singularities of $\Psi_{++}(z_1, \sqrt[k_1^2 - z_1^2]{})$ or $\Psi_{++}(z_1, \sqrt[k_1^2 - z_1^2]{})$ which may hit P in this limit. Now, to recover the physical wave-fields' far-field asymptotics and thus prove the correctness of (4.1), we need to make sense of (1.1) in the limit $\varkappa \rightarrow 0$. Taking this limit is non-trivial, however, and it requires to change the surface \mathbb{R}^2 to another surface Γ , by using the generalised theorem of Stokes, such that Γ does not hit any of the spectral functions' singularities during this limit. We refer to (Shabat, 1991) and (Madsen and Tornehave, 1997) for more on Stokes' theorem. The singularity structure of the spectral functions was thoroughly studied in (Kunz and Assier, 2023), and will be provided in Sections 6, for the simple case, and in Section 7, for the complicated case.

5.2 Obtaining far-field asymptotics

Since we will rely on using the machinery developed in (Assier et al., 2022) in order to recover the physical far-field asymptotics of the scattered and transmitted fields associated to the right-angled no-contrast penetrable wedge diffraction problem, let us briefly summarise this paper's key results.

Consider an integral of the form

$$f(\mathbf{x}; \varkappa) = \frac{1}{4\pi^2} \iint_{\mathbb{R}^2} F(\boldsymbol{\alpha}; \varkappa) e^{-i\mathbf{x} \cdot \boldsymbol{\alpha}} d\boldsymbol{\alpha}, \quad (5.9)$$

where $\varkappa \geq 0$ is some (small) real, positive parameter. For example, $f = \psi$ or $f = \phi_{\text{sc}}$ where $\varkappa = \text{Im}(k_2)$ or $\varkappa = \text{Im}(k_1)$, respectively. Let us assume that the singularity set σ of F consists (only) of poles and branches. We moreover assume that

$$\sigma = \cup_j \sigma_j$$

is the union of so-called *irreducible singularities* σ_j . That is, $\sigma_j = \{\boldsymbol{\alpha} \in \mathbb{C}^2 \mid g_j(\boldsymbol{\alpha}) = 0\}$ is the zero set of some holomorphic function $g_j(\boldsymbol{\alpha})$ such that $(\partial_{\alpha_1} g_j, \partial_{\alpha_2} g_j) \neq 0$ on σ_j . Such g_j is henceforth called a *defining function* of σ_j . The preceding assumptions imply that our irreducible singularities are *regular analytic sets*. For a detailed introduction to the latter, we refer to (Shabat, 1991) and (Chirka, 1989).

The function $F(\boldsymbol{\alpha}; \varkappa)$ is chosen such that, when $\varkappa > 0$, we have $\sigma \cap \mathbb{R}^2 = \emptyset$. However, when $\varkappa \rightarrow 0$, σ hits the real plane at its real trace σ' , which is defined by

$$\sigma' = \sigma \cap \mathbb{R}^2.$$

If it is possible to deform the surface \mathbb{R}^2 continuously to another surface Γ such that $\sigma \cap \Gamma = \emptyset$ for all sufficiently small \varkappa , then, by Stokes' theorem, we can define $f(\mathbf{x}; 0)$ as

$$f(\mathbf{x}; 0) = \frac{1}{4\pi^2} \iint_{\Gamma} F(\boldsymbol{\alpha}; 0) e^{-i\mathbf{x} \cdot \boldsymbol{\alpha}} d\boldsymbol{\alpha}. \quad (5.10)$$

Due to Stokes' theorem, again, this integral is completely determined by the relative position of Γ to σ (as long as no singularities are hit, Γ can be deformed onto any other surface Γ'). This relative position can be described by the bridge and arrow notation, which was first introduced in (Assier and Shanin, 2021b), and further developed in (Assier et al., 2022). Below, we briefly outline its key aspects.

5.2.1 The bridge and arrow notation

We only consider functions with the following *real property*.

Definition 5.1. Let $\sigma = \cup \sigma_j$ where the σ_j are irreducible singularities with respective defining functions g_j . We define

$$\mathbf{a}_j^* = \partial_{\alpha_1} g_j(\boldsymbol{\alpha}^*), \quad \mathbf{b}_j^* = \partial_{\alpha_2} g_j(\boldsymbol{\alpha}^*), \quad (5.11)$$

and say that σ_j has the real property when for every $\boldsymbol{\alpha}^* \in \mathbb{R}^2$, we have $g_j(\boldsymbol{\alpha}^*) \in \mathbb{R}$, $\mathbf{a}_j^* \in \mathbb{R}$, and $\mathbf{b}_j^* \in \mathbb{R}$. Since σ_j is regular, we have $(\mathbf{a}_j^*)^2 + (\mathbf{b}_j^*)^2 \neq 0$. In this case, the real trace $\sigma' = \sigma \cap \mathbb{R}^2$ is a smooth, one dimensional curve.

Let us now discuss how the deformation $\mathbb{R}^2 \rightarrow \Gamma$ can be achieved practically. The following discussion is informal, however, and we refer to (Assier et al., 2022) for a more rigorous formulation of the concepts introduced below.

Since the singularity σ_j depends, generally, on the parameter \varkappa , let us for now write $\sigma_j = \sigma_j(\varkappa)$, and similarly $g_j(\boldsymbol{\alpha}) = g_j(\boldsymbol{\alpha}; \varkappa)$. However, since $\sigma_j' = \sigma_j(0) \cap \mathbb{R}^2$, it does not depend on \varkappa , and we will just write σ_j' without ambiguity.

Let $\boldsymbol{\alpha}^* \in \sigma_j'$. Let us analyse how the integration surface \mathbb{R}^2 needs to be changed for the integral (5.9) to be well-defined in the limit $\varkappa \rightarrow 0$. Without loss of generality, we may assume that $\mathbf{a}_j^* \neq 0$ (if $\mathbf{a}_j^* = 0$, we must have $\mathbf{b}_j^* \neq 0$ and the following procedure can be repeated). Take the complex plane $\{\alpha_2 \equiv \alpha_2^*\} = \{\boldsymbol{\alpha} \in \mathbb{C}^2 \mid \alpha_2 = \alpha_2^*\}$. By the implicit function theorem, there exists a function $\alpha_1^\dagger(\varkappa)$ such that the equation

$$g_j(\alpha_1^\dagger(\varkappa), \alpha_2^*; \varkappa) = 0 \quad (5.12)$$

is solvable for all sufficiently small \varkappa and therefore $\sigma_j(\varkappa) \cap \{\alpha_2 \equiv \alpha_2^*\} = \{(\alpha_1^\dagger(\varkappa), \alpha_2^*)\}$. Clearly, $\{\alpha_2 \equiv \alpha_2^*\} \cap \mathbb{R}^2 = \{\boldsymbol{\alpha} \in \mathbb{R}^2 \mid \alpha_2 = \alpha_2^*\}$ and therefore, the projection of this intersection onto the complex α_1 -plane is simply the real α_1 -line. Since for $\varkappa > 0$, we have $\sigma_j(\varkappa) \cap \mathbb{R}^2 = \emptyset$, the point $\alpha_1^\dagger(\varkappa)$ must have non-zero imaginary part. Therefore, $\alpha_1^\dagger(\varkappa)$ lies either above, or below, the real α_1 line, as illustrated in Fig. 7 (left).

Now, it is possible to continuously change the surface \mathbb{R}^2 to another surface Γ such that, during this change, the singularity $\sigma_j(\varkappa)$ is never hit, for any \varkappa , and such that $\Gamma \cap \sigma_j' = \emptyset$. This is shown in Fig. 7 (centre), where the curve γ is the projection of Γ onto the complex α_1 -plane. For our purpose, it is enough to consider surfaces Γ that can be parametrised over the real plane: Γ can be described by $\{\boldsymbol{\alpha}_\Gamma(\boldsymbol{\alpha}^r) \in \mathbb{C}^2 \mid \boldsymbol{\alpha}^r = (\alpha_1^r, \alpha_2^r) \in \mathbb{R}^2\}$, where

$$\boldsymbol{\alpha}_\Gamma(\boldsymbol{\alpha}^r) = (\alpha_1^r + i\eta_1(\boldsymbol{\alpha}^r), \alpha_2^r + i\eta_2(\boldsymbol{\alpha}^r))$$

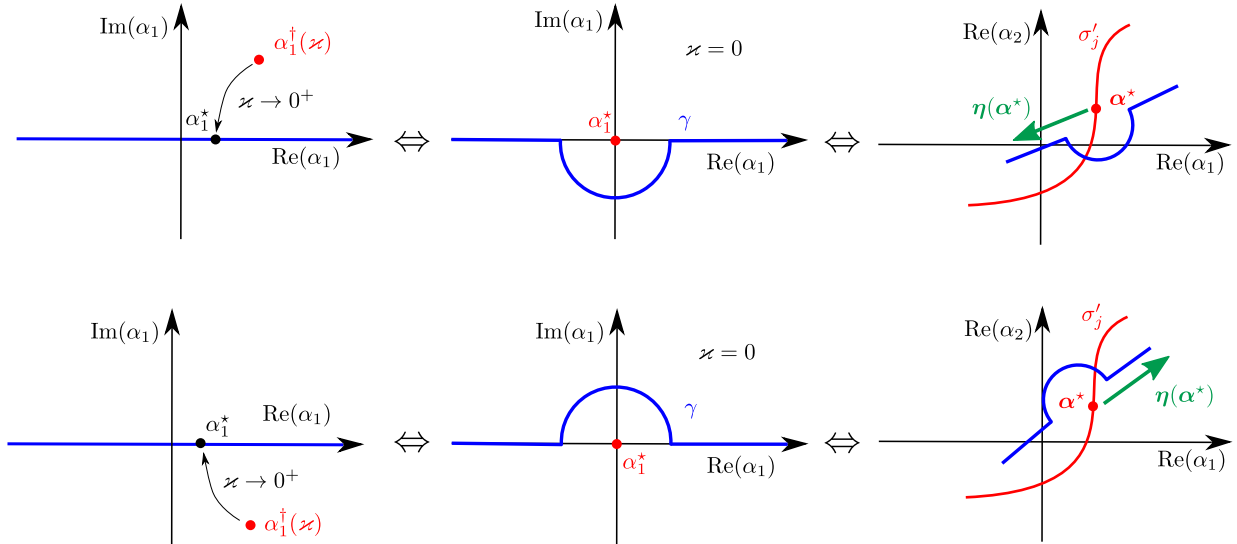


Figure 7: The only two possible types of indentation of the deformed surface Γ about σ_j , and the resulting bridge and arrow configuration.

for some vector field $\eta: \mathbb{R}^2 \rightarrow \mathbb{R}^2$. For Γ to be suitable, we need to choose η such that $\eta(\alpha^*)$, for $\alpha^* \in \sigma'_j$, $\eta(\alpha^*)$ is not tangent to σ'_j and not zero. For a given $\alpha^* \in \sigma'_j$, we call $\eta(\alpha^*)$ the *arrow* at the point α^* . Since η is never tangent to σ'_j , nowhere on σ'_j vanishing, and since σ'_j is a curve in \mathbb{R}^2 , the arrow must point either to the right, or to the left of σ'_j , as illustrated in Fig. 7, right³. It can be shown that if $\alpha_1^\dagger(z)$ lies above the real α_1 -axis, then the arrow points to the left of σ'_j and, similarly, if $\alpha_1^\dagger(z)$ lies below the real α_1 -axis, then the arrow points to the right of σ'_j (see Fig. 7). We refer to (Assier et al., 2022), Section 3 for the proof of all of the above statements.

We can therefore visualise the relative position of Γ to σ_j by using the bridge and arrow symbol, which we ‘attach’ to the singularity’s real trace σ'_j , as shown in Fig. 7 (right).

Notation. Henceforth, we shall omit the argument z whenever $z = 0$.

The bridge and arrow configuration has the crucial, and practically very useful, property that it can be continuously carried along a singularity’s real-trace, as illustrated in Fig. 8. That is, if the arrow points to a given side of σ'_j at one point $\alpha^* \in \sigma'_j$, then it must point to this side at each point $\alpha \in \sigma'_j$. Moreover, we have the following *tangential touch compatibility* (which is also illustrated in Fig. 8). If two singularities σ_1 and σ_2 intersect tangentially at $\alpha_j^* \in \sigma'_1 \cap \sigma'_2$, then the arrow points to the same side of both, σ'_1 and σ'_2 .

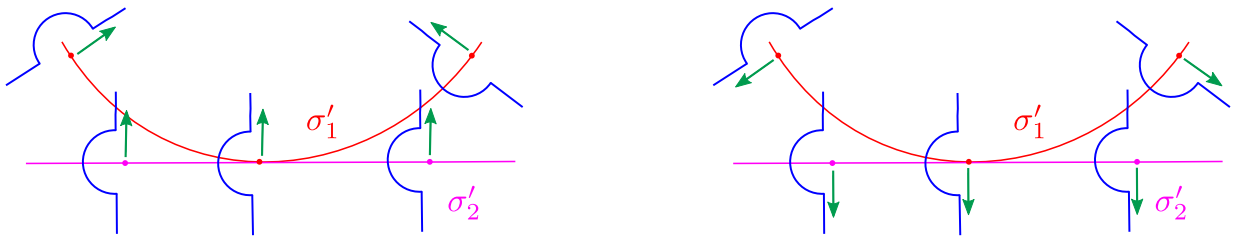


Figure 8: The two possible bridge and arrow configurations for a tangential crossing.

³Here, the notion of ‘left’ and ‘right’ is as follows: right, if for $\alpha_1^\dagger \neq 0$ η is on the same side as the positive $\text{Re}(\alpha_1)$ direction, and left otherwise.

5.2.2 The locality principle

Crucial for estimating integrals of the form (5.9) is the following *locality principle*. This principle relies on the concept of *contributing points*, which we explain after the theorem is stated.

Theorem 5.2 ((Assier et al., 2022) Theorem 6.1). *The integral $f(\mathbf{x})$ can be estimated as $|\mathbf{x}| \rightarrow \infty$ as an asymptotic series. For almost all observation directions $\tilde{\mathbf{x}} = \mathbf{x}/|\mathbf{x}|$, the terms of the asymptotic series (up to terms decaying exponentially as $|\mathbf{x}| \rightarrow \infty$) can be obtained by estimating the integral in the neighbourhoods of some real, isolated, contributing points.*

Contributing points The only potentially contributing points, in the sense of Theorem 5.2, are the so-called ‘saddles on singularities’ and transversal crossings of singularities. We explain the concept of a saddle on a singularity (SOS) below, but first, let us examine what this implies regarding the estimation of f . If the point $\alpha^* \in \sigma'_j$ is not a crossing of singularities and not an SOS, there exists an open neighbourhood $U^* \subset \mathbb{C}^2$ of α^* (which intersects Γ) such that the integral

$$f_{\text{loc}}(\mathbf{x}) = \iint_{\Gamma \cap U^*} F(\alpha) e^{-i\mathbf{x} \cdot \alpha} d\alpha \quad (5.13)$$

decays exponentially as $|\mathbf{x}| \rightarrow \infty$ ⁴. Similarly, $f_{\text{loc}}(\mathbf{x})$ decays exponentially if α^* is a point of tangential crossings of singularities, or if α^* is not singular. Although $f_{\text{loc}}(\mathbf{x})$ depends on the point α^* , it will always be clear which point α^* is referred to, such that this notation is non-ambiguous.

Definition 5.3 (Contributing point). *If $f_{\text{loc}}(\mathbf{x})$ does not decay exponentially, we call α^* a contributing point.*

Definition 5.4 (SOS). *Fix an observation direction $\tilde{\mathbf{x}}$ defined by $\mathbf{x} = r\tilde{\mathbf{x}}$ (i.e. $\tilde{\mathbf{x}} = (\cos(\vartheta), \sin(\vartheta))$). Let $\tilde{\mathbf{x}}$ be orthogonal to σ'_j at the point $\alpha^* \in \sigma'_j$. If the bridge and arrow configuration is such that $\tilde{\mathbf{x}} \cdot \boldsymbol{\eta}(\alpha^*) > 0$, then α^* is called an SOS on σ_j with respect to $\tilde{\mathbf{x}}$.*

Estimation of integrals We now outline how the locality principle can be used in practice. For an irreducible singularity σ_j , let

$$\mathbf{n}_j^* = \frac{1}{\sqrt{(\mathbf{a}_j^*)^2 + (\mathbf{b}_j^*)^2}} \begin{pmatrix} \mathbf{a}_j^* \\ \mathbf{b}_j^* \end{pmatrix}.$$

Transversal crossing of singularities. Let $\alpha^* \in \sigma'_1 \cap \sigma'_2$ and let us assume that the singularities σ_1 and σ_2 cross transversally at α^* . Set $\Delta^* = \mathbf{a}_1^* \mathbf{b}_2^* - \mathbf{a}_2^* \mathbf{b}_1^*$, and let us assume that $\Delta^* > 0$ ⁵. Introduce the sign factors s_1 and s_2 as follows. For $j = 1, 2$, we set $s_j = +1$ (respectively $s_j = -1$), if $\text{sign}(\mathbf{n}_j^* \cdot \boldsymbol{\eta}(\alpha^*)) > 0$ (resp. $\text{sign}(\mathbf{n}_j^* \cdot \boldsymbol{\eta}(\alpha^*)) < 0$). Let $\tilde{\mathbf{x}}$ be such that α^* is not an SOS with respect to $\tilde{\mathbf{x}}$. If there exist constants $A \in \mathbb{C}$ and $m_{1,2} \in \mathbb{R}$ such that

$$F(\alpha) \sim A \times g_1^{-m_1}(\alpha) \times g_2^{-m_2}(\alpha), \text{ as } \alpha \rightarrow \alpha^* \quad (5.14)$$

then, as $r \rightarrow \infty$, we have

$$f_{\text{loc}}(\mathbf{x}) \sim \frac{A e^{-i\mathbf{x} \cdot \alpha^*} e^{-i\frac{\pi}{2}(s_1 m_1 + s_2 m_2)}}{\Gamma(m_1) \Gamma(m_2) (\Delta^*)^{m_1 + m_2 - 1}} \frac{\mathcal{H}(s_1(x_1 \mathbf{b}_2^* - x_2 \mathbf{a}_2^*))}{|x_1 \mathbf{b}_2^* - x_2 \mathbf{a}_2^*|^{1-m_1}} \frac{\mathcal{H}(s_2(-x_1 \mathbf{b}_1^* + x_2 \mathbf{a}_1^*))}{|-x_1 \mathbf{b}_1^* + x_2 \mathbf{a}_1^*|^{1-m_2}}, \quad (5.15)$$

⁴To show this, the integration surface Γ may need to be deformed once more to another surface, Γ' , say, on which $\tilde{\mathbf{x}} \cdot \boldsymbol{\eta}' < 0$. Again, we refer to (Assier et al., 2022) for the technical details involved.

⁵Since the crossing is transversal we always have $\Delta^* \neq 0$, and by eventually changing the sign of the defining function g_1 , say, the condition $\Delta^* > 0$ is non-restrictive.

where \mathcal{H} is the Heaviside step-function, and Γ is the gamma function (see (Assier et al., 2022), Section 5.2). If m_1 or m_2 is a negative integer, no crossing of singularities occurs, and f_{loc} is exponentially decaying.

Isolated SOS. We will only consider *isolated* SOS: in some small open neighbourhood U^* of α^* , the point α^* is the only SOS on σ'_j with respect to $\tilde{\mathbf{x}}$, and α^* does not belong to any other singularity. Similar to the case of a transversal crossing discussed above, we introduce the sign factor s as follows. $s = +1$, if $\text{sign}(\mathbf{n}_j^* \cdot \boldsymbol{\eta}(\alpha^*)) > 0$, and $s = -1$, if $\text{sign}(\mathbf{n}_j^* \cdot \boldsymbol{\eta}(\alpha^*)) < 0$. Let now α^* be an isolated SOS with respect to $\tilde{\mathbf{x}}$. If there exist constants $A \in \mathbb{C}$ and $m \in \mathbb{R}$ such that

$$F(\boldsymbol{\alpha}) \sim A \times g_j^{-m}(\boldsymbol{\alpha}), \text{ as } \boldsymbol{\alpha} \rightarrow \alpha^* \quad (5.16)$$

then, as $r \rightarrow \infty$, we have

$$f_{\text{loc}}(\mathbf{x}) \sim \frac{Ae^{-i\mathbf{x} \cdot \alpha^*} \sqrt{\pi} e^{-ism\pi/2}}{2\pi \left((a_j^*)^2 + (b_j^*)^2 \right) \Gamma(m)} \left(\frac{r}{\sqrt{(a_j^*)^2 + (b_j^*)^2}} \right)^{m-3/2} \times \begin{cases} \frac{e^{-i\pi/4}}{\sqrt{s\xi}} & \text{if } s\xi > 0, \\ \frac{e^{i\pi/4}}{\sqrt{-s\xi}} & \text{if } s\xi < 0, \end{cases} \quad (5.17)$$

see (Assier et al., 2022), Section 5.1 (as in the case of a transversal crossing of singularities, if m is a negative integer, f_{loc} is exponentially decaying). Here, the constant ξ is defined as follows. Set

$$\Lambda = \mathbf{a}^*(\alpha_1 - \alpha_1^*) + \mathbf{b}^*(\alpha_2 - \alpha_2^*), \text{ and } \zeta = \mathbf{b}^*(\alpha_1 - \alpha_1^*) - \mathbf{a}^*(\alpha_2 - \alpha_2^*). \quad (5.18)$$

Then, it can be shown that there exists a unique constant $\xi \in \mathbb{R}$ such that

$$g(\boldsymbol{\alpha}) = \Lambda - \xi\zeta^2 + \mathcal{O}(\Lambda^2 + \zeta\Lambda) \text{ as } \boldsymbol{\alpha} \rightarrow \alpha^*. \quad (5.19)$$

The proof can be found Appendix A of (Assier et al., 2022), and shows that ξ is proportional to the curvature of σ'_j at α^* .

Thus, overall, to obtain the sought asymptotic expansion of f , it is enough to estimate F near the potentially contributing points.

Definition 5.5 (Wave component). *If $f_{\text{loc}}(\mathbf{x})$ is not exponentially decaying, we call the wave-field associated with the leading order far-field asymptotics of $f_{\text{loc}}(\mathbf{x})$, as described by (5.15) and (5.17), a wave component of f .*

Therefore, to prove the correctness of (4.1), we need to show that the wave components of ϕ are given by ϕ_{GO} , ϕ_{C} , ϕ_{L_1} , and ϕ_{L_2} and, similarly, that the wave components of ψ are given by ψ_{GO} , ψ_{C} , ψ_{L_1} , and ψ_{L_2} .

Before we proceed with the corresponding calculation, let us outline the general strategy that we will follow throughout the rest of this article. Let α^* be either a transversal crossing of singularities or an isolated SOS.

Step 0. Determine the bridge and arrow configuration at α^* .

Step 1. Choose defining functions g_1 and g_2 such that $\Delta^* > 0$ (transverse crossing), or some defining function g (SOS). This allows for determining the sign factors and the constant ξ .

Step 2. Study the asymptotic behaviour of $F = \Psi_{++}$ or $F = \Phi_{3/4}$ near α^* , and determine whether $f_{\text{loc}}(\mathbf{x})$ is exponentially decaying.

Step 3. If $f_{\text{loc}}(\mathbf{x})$ does not decay exponentially, use the formulae presented in Section 5.2.2 to obtain the corresponding wave component.

Moreover, the following notation will be used throughout the remainder of this article.

Notation (Contributing asymptotic behaviour). Let F be any function for which the asymptotic behaviour as $\boldsymbol{\alpha} \rightarrow \boldsymbol{\alpha}^*$ is to be found. Let us assume that, as $\boldsymbol{\alpha} \rightarrow \boldsymbol{\alpha}^*$, we have

$$F(\boldsymbol{\alpha}) \sim F_1(\boldsymbol{\alpha}) + F_2(\boldsymbol{\alpha}),$$

and that, depending on whether $\boldsymbol{\alpha}^*$ is an SOS or a point of transversal crossings of singularities, $F_1(\boldsymbol{\alpha})$ has no isolated SOS on $\boldsymbol{\alpha}^*$ (relative to the observation direction $\tilde{\boldsymbol{x}}$ of interest), or $F_1(\boldsymbol{\alpha})$ does not exhibit a transversal crossing of singularities at $\boldsymbol{\alpha}^*$, respectively. We then write

$$F(\boldsymbol{\alpha}) \overset{\text{contr.}}{\sim} F_2(\boldsymbol{\alpha}), \quad \text{as } \boldsymbol{\alpha} \rightarrow \boldsymbol{\alpha}^*.$$

This notation is motivated by the fact, that we are interested in the asymptotic behaviour of

$$f_{\text{loc}}(\boldsymbol{x}) = \frac{1}{4\pi^2} \iint_{\Gamma \cap U^*} F(\boldsymbol{\alpha}) e^{-i\boldsymbol{x} \cdot \boldsymbol{\alpha}} d\boldsymbol{\alpha},$$

and the integral over F_1 must decay exponentially. Since we are only interested in the wave components associated with f_{loc} , the integral over F_1 may thus be discarded. In other words, the *contributing* asymptotic behaviour of F is completely determined by the asymptotic behaviour of F_2 .

6 The simple case

Recall that the ‘simple case’ corresponds to $\vartheta_0 \in (\pi, 3\pi/2)$ where ϑ_0 is the incident angle. In (Kunz and Assier, 2023), it was shown that we then have the following irreducible singularities of Ψ_{++} and $\Phi_{3/4}$.

$$\begin{aligned} \sigma_{p_1} &= \{\boldsymbol{\alpha} \in \mathbb{C}^2 \mid \alpha_1 = \mathbf{a}_1\}, \quad \sigma_{p_2} = \{\boldsymbol{\alpha} \in \mathbb{C}^2 \mid \alpha_1 = \mathbf{a}_2\}, \quad \sigma_{b_1} = \{\boldsymbol{\alpha} \in \mathbb{C}^2 \mid \alpha_1 = -k_1\}, \\ \sigma_{b_2} &= \{\boldsymbol{\alpha} \in \mathbb{C}^2 \mid \alpha_1 = -k_2\}, \quad \sigma_{b_3} = \{\boldsymbol{\alpha} \in \mathbb{C}^2 \mid \alpha_2 = -k_1\}, \quad \sigma_{b_4} = \{\boldsymbol{\alpha} \in \mathbb{C}^2 \mid \alpha_2 = -k_2\}. \end{aligned}$$

The subscript p indicates a polar singularity, whereas the subscript b denotes a branch. Here, the assumption that $\vartheta_0 \neq \pi, 3\pi/2$ is important, since it ensures that the polar and branch sets are not coalescing. Moreover, the set σ_{c_1} , introduced below, is an irreducible polar singularity of $\Phi_{3/4}$ whereas the set σ_{c_2} is an irreducible polar singularity of Ψ_{++} .

$$\sigma_{c_1} = \{\boldsymbol{\alpha} \in \mathbb{C}^2 \mid \alpha_1^2 + \alpha_2^2 = k_1^2\}, \quad \sigma_{c_2} = \{\boldsymbol{\alpha} \in \mathbb{C}^2 \mid \alpha_1^2 + \alpha_2^2 = k_2^2\}.$$

Observe that all of these irreducible singularities are regular and have the real property. Their real traces are shown in Fig. 9. Thus, the framework outlined in Section 5.2 is indeed applicable. In (Kunz and Assier, 2023), it was shown that only parts of σ_{c_1} and σ_{c_2} are actually singular. This is why we only show parts of the circles in Fig. 9. Now, using the procedure described in Section 3 of (Assier et al., 2022) (which is summarised in Section 5.2.1), it is reasonably straightforward to find the bridge and arrow configuration on the sets $\sigma'_{p_j}, j = 1, 2$ and $\sigma'_{b_j}, j = 1, 2, 3, 4$. Then, by tangential-touch compatibility, the bridge and arrow configuration can be found on σ'_{c_1} and σ'_{c_2} . The resulting configurations are shown in Fig. 9.

Henceforth, let $\boldsymbol{x} = r\tilde{\boldsymbol{x}}$ with $\tilde{\boldsymbol{x}} = (\cos(\vartheta), \sin(\vartheta))$, and let us assume that $\vartheta \neq 0, \pi/2$. Recall that the only points that can potentially yield wave components are transversal crossings of singularities and SOS. Since $\vartheta \neq 0, \pi/2$, only points on σ'_{c_1} and σ'_{c_2} , respectively, can be such an SOS. We proceed by studying these potentially contributing points. Recall that, we only consider $k_1 \neq k_2$ for, otherwise, the penetrable wedge diffraction problem described in Section 2 is trivial.

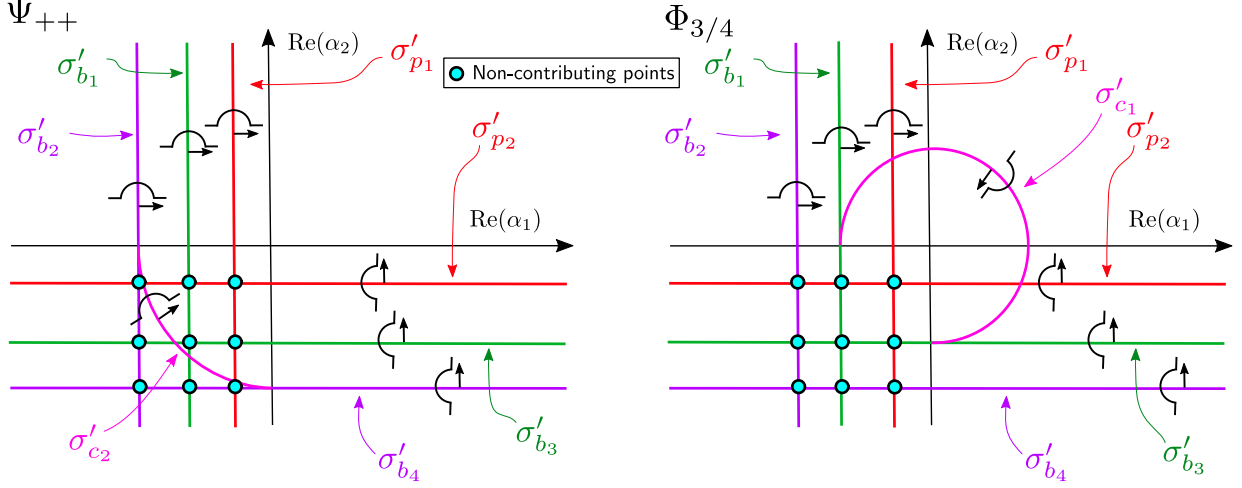


Figure 9: Real traces of the spectral functions' irreducible singularities, corresponding bridge and arrow configuration, and non-contributing points.

6.1 Non-contributing crossings

In this section, we look at all crossings that do not involve the circles σ'_{c_1} and σ'_{c_2} . That is, we analyse the crossings $\sigma'_{p_1} \cap \sigma'_{p_2}$, $\sigma'_{p_j} \cap \sigma'_{b_l}$, $j = 1, 2$; $l = 1, 2, 3, 4$ and $\sigma'_{b_j} \cap \sigma'_{b_l}$, $j, l = 1, 2, 3, 4$. In Section 4 of (Kunz and Assier, 2023), it was shown that the crossings $\sigma'_{b_j} \cap \sigma'_{b_l}$, $j, l = 1, 2, 3, 4$ are ‘additive’ in the sense, that $\Phi_{3/4}$ satisfies the additive crossing property relative to these crossing points (we refer to (Assier and Shanin, 2019), (Assier et al., 2022), or (Kunz and Assier, 2023) for an explanation of this property). Using the Wiener-Hopf equation (5.1), it can be shown that the spectral function Ψ_{++} also satisfies the additive crossing property relative to these crossings. By Theorem 4.13 of (Assier et al., 2022), such crossings therefore do not yield a wave component. Now, it can be shown that, in fact, all of the crossings highlighted in Fig. 9 are non-contributing, which implies that they do not yield a wave component. The procedure for proving this is the same for each crossing, however, and we therefore only give the proof for the point $\alpha^* = (-k_1, \mathbf{a}_2)$, corresponding to the crossing of σ'_{b_1} and σ'_{p_2} .

Lemma 6.1. *The point $\alpha^* = (-k_1, \mathbf{a}_2)$ is non-contributing.*

Proof. We follow the strategy outlined at the end of Section 5.2.2, and show that α^* is non-contributing for $\Phi = -\Phi_{3/4} - P_{++}$. This implies the sought non-contributing behaviour of Ψ_{++} (by the Wiener-Hopf equation) and of $\Phi_{3/4}$ (since P_{++} does not exhibit a crossing of singularities at α^*). Let $\sigma_1 = \sigma_{b_1}$ and $\sigma_2 = \sigma_{p_2}$.

Step 1. Choose $g_1(\alpha) = \alpha_1 + k_1$ and $g_2(\alpha) = \alpha_2 - \mathbf{a}_2$ as defining functions for the singularities σ_1 and σ_2 , respectively.

Step 2. For $\varkappa > 0$, we have $(-k_1, \mathbf{a}_2) \in \text{LHP} \times \text{LHP}$, so we can use equation (5.5) or (5.6) for computing the asymptotic behaviour of Φ as $\alpha \rightarrow \alpha^*$. Let us use formula (5.5), wherein only the external additive term exhibits a crossing of singularities. Therefore, as $\alpha \rightarrow \alpha^*$, we find

$$-\Phi(\alpha) \stackrel{\text{contr.}}{\sim} \frac{K_{o-}(\alpha)K_{-o}(-k_1, \mathbf{a}_2)}{K_{o-}(\alpha_1, \mathbf{a}_2)K_{-o}(\mathbf{a}_1, \mathbf{a}_2)(-k_1 - \mathbf{a}_1)(\alpha_2 - \mathbf{a}_2)}. \quad (6.1)$$

Now, using the definition of K_{o-} (cf. (5.7)), we have, as $\alpha \rightarrow \alpha^*$

$$\frac{K_{o-}(\alpha)}{K_{o-}(\alpha_1, \mathbf{a}_2)} = \frac{\sqrt[k_2^2 - \alpha_1^2 - \alpha_2]{k_2^2 - \alpha_1^2 - \alpha_2}}{\sqrt[k_1^2 - \alpha_1^2 - \alpha_2]{k_1^2 - \alpha_1^2 - \alpha_2}} \frac{\sqrt[k_1^2 - \alpha_1^2 - \alpha_2]{k_1^2 - \alpha_1^2 - \alpha_2}}{\sqrt[k_2^2 - \alpha_1^2 - \alpha_2]{k_2^2 - \alpha_1^2 - \alpha_2}} \sim \frac{\sqrt[k_1^2 - \alpha_1^2 - \alpha_2]{k_1^2 - \alpha_1^2 - \alpha_2}}{\sqrt[k_1^2 - \alpha_1^2 - \alpha_2]{k_1^2 - \alpha_1^2 - \alpha_2}}, \quad (6.2)$$

and, moreover, we have

$$\frac{\sqrt[k_1^2 - \alpha_1^2]{k_1^2 - \alpha_1^2 - \mathbf{a}_2}}{\sqrt[k_1^2 - \alpha_1^2]{k_1^2 - \alpha_1^2 - \alpha_2}} = \frac{k_1^2 - \alpha_1^2 - \mathbf{a}_2 \alpha_2}{k_1^2 - \alpha_1^2 - \alpha_2^2} + \frac{\sqrt[k_1^2 - \alpha_1^2]{k_1^2 - \alpha_1^2}(\alpha_2 - \mathbf{a}_2)}{k_1^2 - \alpha_1^2 - \alpha_2^2}. \quad (6.3)$$

Therefore, as $\boldsymbol{\alpha} \rightarrow \boldsymbol{\alpha}^*$, we find

$$-\Phi(\boldsymbol{\alpha}) \stackrel{\text{contr.}}{\sim} \underbrace{\frac{K_{-\circ}(-k_1, \mathbf{a}_2)}{K_{-\circ}(\mathbf{a}_1, \mathbf{a}_2)(-k_1 - \mathbf{a}_1)(\alpha_2 - \mathbf{a}_2)}}_{U_1(\boldsymbol{\alpha})} + \underbrace{\frac{K_{-\circ}(-k_1, \mathbf{a}_2) \sqrt[k_1^2 - \alpha_1^2]{k_1^2 - \alpha_1^2}}{K_{-\circ}(\mathbf{a}_1, \mathbf{a}_2)(-k_1 - \mathbf{a}_1)(-\alpha_2^2)}}_{U_2(\boldsymbol{\alpha})}. \quad (6.4)$$

Now, the first term, $U_1(\boldsymbol{\alpha})$, is regular at $\alpha_1 = -k_1$ whereas the second term, $U_2(\boldsymbol{\alpha})$, is regular at $\alpha_2 = \mathbf{a}_2$. Therefore, neither U_1 nor U_2 exhibits a crossing of singularities at $\boldsymbol{\alpha} = \boldsymbol{\alpha}^*$ and thus, the crossing is additive. Therefore, by Theorem 4.13 of (Assier et al., 2022), it does not lead to a wave component. \square

Remark 6.2. Analysing the crossing $(\mathbf{a}_1, \mathbf{a}_2)$ of σ_{p_1} and σ_{p_2} is slightly different, but easier: proceeding as in the proof of Lemma 6.1, we find that $\Phi \stackrel{\text{contr.}}{\sim} P_{+++}$. This means that the crossing $(\mathbf{a}_1, \mathbf{a}_2)$ is not additive for Φ . However we get $\Phi_{3/4} \stackrel{\text{contr.}}{\sim} 0$, so the crossing does not yield a wave component.

6.2 Wave components of ψ

Let us now study the remaining transversal crossings as well as the points which are isolated SOS of Ψ_{+++} . Recall that $\tilde{\mathbf{x}} = (\cos(\vartheta), \sin(\vartheta))$. When $k_2 < k_1$, the remaining potentially contributing points of Ψ_{+++} are given by

$$\boldsymbol{\alpha}_{T_1} = \left(-\sqrt{k_2^2 - \mathbf{a}_2^2}, \mathbf{a}_2 \right), \quad \boldsymbol{\alpha}_{T_2} = \left(\mathbf{a}_1, -\sqrt{k_2^2 - \mathbf{a}_1^2} \right), \quad \boldsymbol{\alpha}_{C_2}(\vartheta) = -k_2 \tilde{\mathbf{x}}$$

and when $k_2 > k_1$, we obtain the additional contributing points

$$\boldsymbol{\alpha}_{L_1} = \left(\sqrt{k_2^2 - k_1^2}, -k_1 \right), \quad \boldsymbol{\alpha}_{L_2} = \left(-k_1, -\sqrt{k_2^2 - k_1^2} \right),$$

as illustrated in Fig. 10. The bridge and arrow configuration at these contributing points is as displayed in Fig. 9.

6.2.1 The transmitted waves

Since the wave components corresponding to the points $\boldsymbol{\alpha}_{T_1}$ and $\boldsymbol{\alpha}_{T_2}$ are computed similarly, we will only do it in detail for the wave corresponding to the point $\boldsymbol{\alpha}_{T_1}$. We refer to (Kunz, 2023) for a more detailed discussion. We henceforth assume that $k_2^2 - \mathbf{a}_2^2 \geq 0$, for otherwise $\boldsymbol{\alpha}_{T_1} \notin \mathbb{R}^2$. In this case, we obtain no corresponding wave component, which corresponds to total (internal) reflection of ϕ_{in} on the wedge's face $\{x_1 = 0, x_2 > 0\}$. Similarly, we assume $k_2^2 - \mathbf{a}_1^2 \geq 0$, for $k_2^2 - \mathbf{a}_1^2 < 0$ corresponds to total (internal) reflection of ϕ_{in} on the wedge's face $\{x_1 > 0, x_2 = 0\}$.

The transmitted wave ψ_{T_1} . Let us consider the contribution of the point $\boldsymbol{\alpha}^* = \boldsymbol{\alpha}_{T_1}$, which is a transverse crossing of σ'_{p_2} and σ'_{c_2} . The corresponding bridge and arrow configuration is displayed in Fig. 9. Let $\sigma_1 = \sigma_{c_2}$ and $\sigma_2 = \sigma_{p_2}$.

Step 1. Choose $g_1(\boldsymbol{\alpha}) = k_2^2 - \alpha_1^2 - \alpha_2^2$ and $g_2(\boldsymbol{\alpha}) = \alpha_2 - \mathbf{a}_2$. Due to the bridge and arrow configuration at $\sigma'_1 \cap \sigma'_2$ and since $\mathbf{n}_1^* = -\mathbf{e}_r$, and $\mathbf{n}_2^* = \mathbf{e}_{\text{Re}(\alpha_2)}$, the sign factors are given by $s_1 = s_2 = +1$.

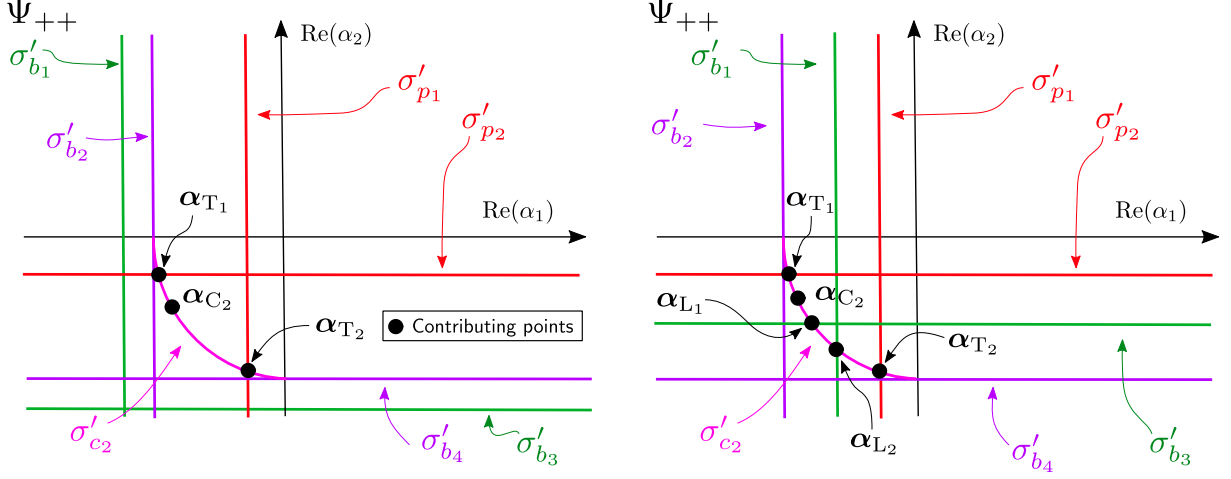


Figure 10: Contributing points of Ψ_{++} for $k_2 < k_1$ (left) and $k_2 > k_1$ (right).

Step 2. For $\varkappa > 0$, we have $\alpha_{T_1} \in \text{LHP} \times \text{LHP}$, and we use (5.6) for computing the asymptotic behaviour of Ψ_{++} as $\alpha \rightarrow \alpha_{T_1}$. Now, only the external additive term in equation (5.5) contributes to the far-field since the integral term does not exhibit a crossing of singularities at α_{T_1} . Therefore

$$\begin{aligned} \Psi_{++}(\alpha) &\stackrel{\text{contr.}}{\sim} -\frac{K_{-\circ}(\alpha)(k_1^2 - \alpha_1^2 - \alpha_2^2)}{K_{-\circ}(\mathbf{a}_1, \mathbf{a}_2)(\alpha_1 - \mathbf{a}_1)} \frac{1}{(\alpha_2 - \mathbf{a}_2)(k_2^2 - \alpha_1^2 - \alpha_2^2)} \\ &\sim \frac{4\mathbf{a}_1 \sqrt{k_2^2 - \mathbf{a}_2^2}}{\sqrt{k_2^2 - \mathbf{a}_2 - \mathbf{a}_1}} \frac{1}{(\alpha_2 - \mathbf{a}_2)(k_2^2 - \alpha_1^2 - \alpha_2^2)}, \end{aligned} \quad (6.5)$$

which is exactly of the form

$$\Psi_{++}(\alpha) \sim A \times g_1(\alpha)^{-m_1} \times g_2(\alpha)^{-m_2}$$

for

$$A = \frac{4\mathbf{a}_1 \sqrt{k_2^2 - \mathbf{a}_2^2}}{\sqrt{k_2^2 - \mathbf{a}_2 - \mathbf{a}_1}}, \quad \text{and} \quad m_1 = m_2 = 1.$$

Step 3. We can now use equation (5.15) to obtain the wave component ψ_{T_1} corresponding to the crossing α_{T_1} , and find

$$\psi_{T_1}(\mathbf{x}) = \frac{2\mathbf{a}_1}{\mathbf{a}_1 - \sqrt{k_2^2 - \mathbf{a}_2^2}} e^{-i(-x_1 \sqrt{k_2^2 - \mathbf{a}_2^2} + x_2 \mathbf{a}_2)} \mathcal{H}(x_1) \mathcal{H}\left(x_1 \mathbf{a}_2 + x_2 \sqrt{k_2^2 - \mathbf{a}_2^2}\right). \quad (6.6)$$

The transmitted wave ψ_{T_2} . Now consider the point $\alpha^* = \alpha_{T_2}$. The corresponding wave component is computed similarly: it is again sufficient to only analyse (5.5)'s external additive term and, again, we can use (5.15) to find the wave component ψ_{T_2} corresponding to the crossing α_{T_2} . This yields

$$\psi_{T_2}(\mathbf{x}) = \frac{2\mathbf{a}_2}{\mathbf{a}_2 - \sqrt{k_2^2 - \mathbf{a}_1^2}} e^{-i(x_1 \mathbf{a}_1 - x_2 \sqrt{k_2^2 - \mathbf{a}_1^2})} \mathcal{H}\left(x_1 \sqrt{k_2^2 - \mathbf{a}_1^2} + x_2 \mathbf{a}_1\right) \mathcal{H}(x_2). \quad (6.7)$$

The fields ψ_{T_1} and ψ_{T_2} are in perfect agreement with the corresponding wave-fields that are predicted by GO, and which are illustrated in Fig. 4.

6.2.2 The cylindrical diffracted wave

Next, we investigate the contributing behaviour of Ψ_{++} near $\boldsymbol{\alpha}^* = \boldsymbol{\alpha}_{C_2}(\vartheta) = -k_2 \tilde{\boldsymbol{x}}$, which is an isolated SOS on σ'_{c_2} with respect to $\tilde{\boldsymbol{x}}$. The bridge and arrow configuration corresponding to this SOS is displayed in Fig. 9.

Step 1. Choose $g(\boldsymbol{\alpha}) = k_2^2 - \alpha_1^2 - \alpha_2^2$ as the defining function for σ_{c_2} . By (Assier et al., 2022) Appendix A, we then find $\xi = 1/(4k_2^2)$, where ξ is the constant introduced in Section 5.2.2. Since $\tilde{\boldsymbol{x}} = \boldsymbol{n}^*$, and since the bridge and arrow configuration is as displayed in Fig. 9, the sign factor is given by $s = +1$.

Step 2. To compute the asymptotic behaviour of Ψ_{++} as $\boldsymbol{\alpha} \rightarrow \boldsymbol{\alpha}_{C_2}(\vartheta)$, we use the fact that $\Psi_{++} = \Phi/K$, where $\Phi = -\Phi_{3/4} - P_{++}$, and that Φ is regular at $\boldsymbol{\alpha}_{C_2}(\vartheta)$, as can be seen from Fig. 9. Thus, as $\boldsymbol{\alpha} \rightarrow \boldsymbol{\alpha}_{C_2}(\vartheta)$, we have

$$\Psi_{++}(\boldsymbol{\alpha}) \sim \Phi(\boldsymbol{\alpha}_{C_2}(\vartheta)) \frac{k_1^2 - k_2^2}{k_2^2 - \alpha_1^2 - \alpha_2^2} \quad (6.8)$$

which is exactly of the form

$$\Psi_{++}(\boldsymbol{\alpha}) \sim A \times g(\boldsymbol{\alpha})^{-m}$$

for

$$A = \Phi(\boldsymbol{\alpha}_{C_2}(\vartheta)) (k_1^2 - k_2^2), \quad \text{and} \quad m = 1.$$

Step 3. We can now use equation (5.17) and find that the wave component ψ_C corresponding to $\boldsymbol{\alpha}_{C_2}(\vartheta)$ is given by

$$\psi_C(r, \vartheta) = \frac{\Phi(k_2 \cos(\vartheta), k_2 \sin(\vartheta))}{8\sqrt{2\pi}} \left(\frac{k_1^2}{k_2^2} - 1 \right) e^{-i3\pi/4} \times \frac{e^{-ik_2 r}}{\sqrt{k_2 r}}, \quad (6.9)$$

which is supported only for $\vartheta \in (0, \pi/2)$. The quantity

$$D_{\psi_C}(\vartheta, \vartheta_0) = \frac{\Phi(k_2 \cos(\vartheta), k_2 \sin(\vartheta))}{8\sqrt{2\pi}} \left(\frac{k_1^2}{k_2^2} - 1 \right) e^{-i3\pi/4} \quad (6.10)$$

corresponds to the (cylindrical) *diffraction coefficient* of ψ .

6.2.3 The lateral diffracted waves

When $k_2 > k_1$, the waves ψ_{T_1} , ψ_{T_2} , and ψ_{C_2} are the only wave components of ψ . However, when $k_1 < k_2$, we obtain two additional waves corresponding to the contributing points $\boldsymbol{\alpha}_{L_1}$ and $\boldsymbol{\alpha}_{L_2}$, as shown in Fig. 10, right. Thus, let $k_1 < k_2$. Moreover, let us assume that $k_1 \neq \sqrt{2}k_2$, for if $k_1 = \sqrt{2}k_2$, the points $\boldsymbol{\alpha}_{L_2}$ and $\boldsymbol{\alpha}_{L_1}$ coalesce, thereby leading to a triple crossing of singularities. We expect that the formulae derived in this Section remain valid in this case, but the detailed study of this will be the basis for future work.

The lateral wave ψ_{L_2} . We begin by studying the contributing behaviour of Ψ_{++} near the point $\boldsymbol{\alpha}^* = \boldsymbol{\alpha}_{L_2}$, which is a transverse crossing of σ'_{b_1} and σ'_{c_2} , with bridge and arrow configuration as displayed in Fig. 9. Let $\sigma_1 = \sigma_{b_1}$ and $\sigma_2 = \sigma_{c_2}$.

Step 1. Choose $g_1(\boldsymbol{\alpha}) = \alpha_1$ and $g_2(\boldsymbol{\alpha}) = k_2^2 - \alpha_1^2 - \alpha_2^2$. As before, the sign factors are given by $s_1 = s_2 = +1$.

Step 2. For $\varkappa > 0$, we have $\boldsymbol{\alpha}_{L_2} \in \text{LHP} \times \text{LHP}$. However, since the integral terms in formulae (5.5) and (5.6) are singular at $\boldsymbol{\alpha}_{L_2}$, we cannot simply study the contributing behaviour of these

formulae's additive terms, but instead the integral terms need to be accounted for as well. This turns out to be easiest when using formula (5.6), wherein the integral term exhibits a polar singularity as $\alpha_1 \rightarrow -k_1$. Therefore, we need to modify formula (5.6) to study this limit. To this end let us assume that α is close to α_{L_2} , and change the contour P in (5.6) to some contour P' as illustrated in Fig. 11. This picks up a residue of the integrand in (5.6) relative to counter-

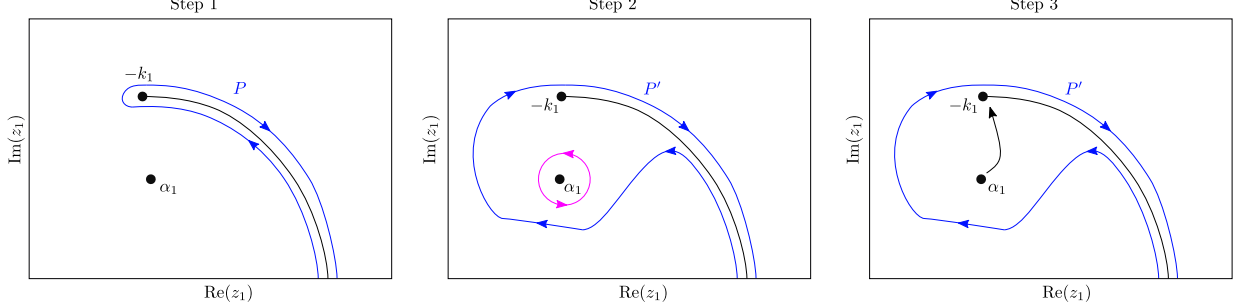


Figure 11: Contour change that modifies equation (5.6) to allow for taking the limit $\alpha_1 \rightarrow -k_1$.

clockwise orientation. Overall, we then obtain

$$\begin{aligned} \Psi_{++}(\alpha) = & \frac{-i}{4\pi K_{+o}(\alpha)} \int_{P'} \mathcal{I}_1(\alpha; z_1) dz_1 + \frac{1}{2K(\alpha)} \left(\frac{(k_2^2 - k_1^2) \Psi_{++}(\alpha_1, \sqrt[3]{k_1^2 - \alpha_1^2})}{\left(\sqrt[3]{k_1^2 - \alpha_1^2} - \alpha_2 \right) \sqrt[3]{k_1^2 - \alpha_1^2}} \right) \\ & - \frac{K_{o-}(\mathbf{a}_1, \mathbf{a}_2) P_{++}(\alpha)}{K_{+o}(\alpha) K_{-o}(\mathbf{a}_1, \mathbf{a}_2) K_{o-}(\mathbf{a}_1, \mathbf{a}_2)}. \end{aligned} \quad (6.11)$$

Now, the integral term as well as the second additive term in (6.11) does not exhibit a crossing of singularities at $\alpha = \alpha_{L_2}$ and therefore, as $\alpha \rightarrow \alpha_{L_2}$, we obtain

$$\Psi_{++}(\alpha) \overset{\text{contr.}}{\sim} \frac{1}{2K(\alpha)} \left(\frac{(k_2^2 - k_1^2) \Psi_{++}(\alpha_1, \sqrt[3]{k_1^2 - \alpha_1^2})}{\left(\sqrt[3]{k_1^2 - \alpha_1^2} - \alpha_2 \right) \sqrt[3]{k_1^2 - \alpha_1^2}} \right). \quad (6.12)$$

Let us now analyse the behaviour of $\Psi_{++}(\alpha_1, \sqrt[3]{k_1^2 - \alpha_1^2})$ as $\alpha_1 \rightarrow -k_1$. Since for $\varkappa > 0$ we have $(\alpha_1, \sqrt[3]{k_1^2 - \alpha_1^2}) \in \text{LHP} \times \text{UHP}$, we need to use (5.5) to analyse this limit, so

$$\begin{aligned} K_{o+}(\alpha_1, \sqrt[3]{k_1^2 - \alpha_1^2}) \Psi_{++}(\alpha_1, \sqrt[3]{k_1^2 - \alpha_1^2}) = & \frac{-i}{4\pi} \int_P \mathcal{I}_2(\alpha_1, \sqrt[3]{k_1^2 - \alpha_1^2}; z_2) dz_2 \\ & - \frac{K_{-o}(\alpha_1, \mathbf{a}_2) P_{++}(\alpha_1, \sqrt[3]{k_1^2 - \alpha_1^2})}{K_{o-}(\alpha_1, \mathbf{a}_2) K_{-o}(\mathbf{a}_1, \mathbf{a}_2)}. \end{aligned} \quad (6.13)$$

Now, using (5.4), one can show that the term on the right hand side of (6.13) is regular as $\alpha_1 \rightarrow -k_1$. We can hence define the quantity $\mathcal{L}_{\psi_{L_2}}(\vartheta_0)$ by

$$\mathcal{L}_{\psi_{L_2}}(\vartheta_0) = \lim_{\alpha_1 \rightarrow -k_1} \left(K_{o+}(\alpha_1, \sqrt[3]{k_1^2 - \alpha_1^2}) \Psi_{++}(\alpha_1, \sqrt[3]{k_1^2 - \alpha_1^2}) \right). \quad (6.14)$$

Note that, $\mathcal{L}_{\psi_{L_2}}(\vartheta_0)$ depends on the incident angle ϑ_0 , since the spectral function Ψ_{++} exhibits this dependence (although it has been suppressed for brevity).

We therefore obtain, as $\alpha_1 \rightarrow -k_1$,

$$\Psi_{++} \left(\alpha_1, \sqrt[3]{k_1^2 - \alpha_1^2} \right) \sim \frac{\mathcal{L}_{\psi_{L_2}}(\vartheta_0)}{K_{\circ+} \left(\alpha_1, \sqrt[3]{k_1^2 - \alpha_1^2} \right)}, \quad (6.15)$$

and thus, as $\boldsymbol{\alpha} \rightarrow \boldsymbol{\alpha}_{L_2}$, we find from (6.12) that

$$\Psi_{++}(\boldsymbol{\alpha}) \stackrel{\text{contr.}}{\sim} \frac{1}{2K(\boldsymbol{\alpha})} \left(\frac{(k_2^2 - k_1^2)}{\left(\sqrt[3]{k_1^2 - \alpha_1^2} - \alpha_2 \right) \sqrt[3]{k_1^2 - \alpha_1^2} K_{\circ+} \left(\alpha_1, \sqrt[3]{k_1^2 - \alpha_1^2} \right)} \frac{\mathcal{L}_{\psi_{L_2}}(\vartheta_0)}{\left(\alpha_1, \sqrt[3]{k_1^2 - \alpha_1^2} \right)} \right). \quad (6.16)$$

Now, a lengthy but straightforward computation shows that

$$\frac{(k_2^2 - k_1^2)}{\left(\sqrt[3]{k_1^2 - \alpha_1^2} - \alpha_2 \right) \sqrt[3]{k_1^2 - \alpha_1^2} K_{\circ+} \left(\alpha_1, \sqrt[3]{k_1^2 - \alpha_1^2} \right)} \stackrel{\text{contr.}}{\sim} \frac{-4 \sqrt[3]{k_2^2 - k_1^2} \sqrt{2k_1} \sqrt[3]{k_1 + \alpha_1}}{k_2^2 - k_1^2} \quad (6.17)$$

and therefore, we find

$$\Psi_{++}(\boldsymbol{\alpha}) \stackrel{\text{contr.}}{\sim} 2 \sqrt{k_2^2 - k_1^2} \sqrt{2k_1} \mathcal{L}_{\psi_{L_2}}(\vartheta_0) \times \frac{g_1(\boldsymbol{\alpha})^{1/2}}{g_2(\boldsymbol{\alpha})}. \quad (6.18)$$

This is exactly of the form

$$\Psi_{++}(\boldsymbol{\alpha}) \stackrel{\text{contr.}}{\sim} A \times g_1(\boldsymbol{\alpha})^{-m_1} \times g_2(\boldsymbol{\alpha})^{-m_2}$$

with $m_1 = -1/2$, $m_2 = 1$, and

$$A = 2 \sqrt{k_2^2 - k_1^2} \sqrt{2k_1} \mathcal{L}_{\psi_{L_2}}(\vartheta_0).$$

Step 3. Let us introduce the *lateral diffraction coefficient*

$$D_{\psi_{L_2}}(\vartheta_0) = \frac{2(k_2^2 - k_1^2)^{3/4} \sqrt{k_1} e^{i3\pi/4} \mathcal{L}_{\psi_{L_2}}(\vartheta_0)}{\sqrt{\pi}}.$$

Then, using (5.15) to obtain the wave component ψ_{L_2} corresponding to the crossing at $\boldsymbol{\alpha}_{L_2}$, we find that

$$\psi_{L_2}(\boldsymbol{x}) = D_{\psi_{L_2}}(\vartheta_0) \frac{e^{i(k_1 x_1 + \sqrt{k_2^2 - k_1^2} x_2)}}{|x_1 \sqrt{k_2^2 - k_1^2} - x_2 k_1|^{3/2}} \mathcal{H} \left(\sqrt{k_2^2 - k_1^2} x_1 - k_1 x_2 \right) \mathcal{H}(x_2). \quad (6.19)$$

The lateral wave ψ_{L_1} . We now consider the point $\boldsymbol{\alpha}^* = \boldsymbol{\alpha}_{L_1}$. Using formula (5.5) to obtain the contributing asymptotic behaviour of Ψ_{++} as $\boldsymbol{\alpha} \rightarrow \boldsymbol{\alpha}_{L_1}$, all corresponding computations are analogous to those carried out previously for the point $\boldsymbol{\alpha}_{L_2}$, so we only give the result. Again, we refer to (Kunz, 2023) for a more detailed discussion. Particularly, we find that the function $K_{+\circ}(\sqrt[3]{k_1^2 - \alpha_2^2}, \alpha_2) \Psi_{++}(\sqrt[3]{k_1^2 - \alpha_2^2}, \alpha_2)$ is regular as $\alpha_2 \rightarrow -k_1$, and we can hence define the quantity $\mathcal{L}_{\psi_{L_1}}(\vartheta_0)$ via

$$\mathcal{L}_{\psi_{L_1}}(\vartheta_0) = \lim_{\alpha_2 \rightarrow -k_1} \left(K_{+\circ} \left(\sqrt[3]{k_1^2 - \alpha_2^2}, \alpha_2 \right) \Psi_{++} \left(\sqrt[3]{k_1^2 - \alpha_2^2}, \alpha_2 \right) \right). \quad (6.20)$$

Then, upon introducing the lateral diffraction coefficient

$$D_{\psi_{L_1}}(\vartheta_0) = \frac{2(k_2^2 - k_1^2)^{3/4} \sqrt{k_1} e^{i3\pi/4} \mathcal{L}_{\psi_{L_1}}(\vartheta_0)}{\sqrt{\pi}}$$

we find that

$$\psi_{L_1}(\mathbf{x}) = D_{\psi_{L_1}}(\vartheta_0) \frac{e^{i(\sqrt{k_2^2 - k_1^2}x_1 + k_1x_2)}}{|x_2 \sqrt{k_2^2 - k_1^2} - x_1 k_1|^{3/2}} \mathcal{H}\left(k_1x_1 - \sqrt{k_2^2 - k_1^2}x_2\right) \mathcal{H}(x_1). \quad (6.21)$$

Formulae (6.19) and (6.21) are in perfect agreement with the form of lateral waves we expect from the studies outlined in Section 4.1. When $k_2 < k_1$, we set $\psi_{L_1} = \psi_{L_2} \equiv 0$.

6.3 Wave components of ϕ

We now proceed to study the remaining transversal crossings as well as the points which are isolated SOS of $\Phi_{3/4}$. When $k_1 < k_2$, these (potentially) contributing points are given by

$$\alpha_{R_1} = \left(-\sqrt{k_1^2 - a_2}, a_2\right), \quad \alpha_{R_2} = \left(a_1, \sqrt{k_1^2 - a_1^2}\right), \quad \alpha_{C_1}(\tilde{\mathbf{x}}) = -k_1 \tilde{\mathbf{x}},$$

and, when $k_1 > k_2$, we obtain the additional contributing points

$$\alpha_{L_1} = \left(-k_2, \sqrt{k_1^2 - k_2^2}\right), \quad \alpha_{L_2} = \left(\sqrt{k_1^2 - k_2^2}, -k_2\right).$$

These points are shown in Fig. 12, and the corresponding bridge and arrow configurations are as displayed in Fig. 9. Here, we have re-used the notation α_{L_1} and α_{L_2} , which we already used for crossings of singularities of Ψ_{++} . The rationale for this choice will be explained in Section 6.3.3.

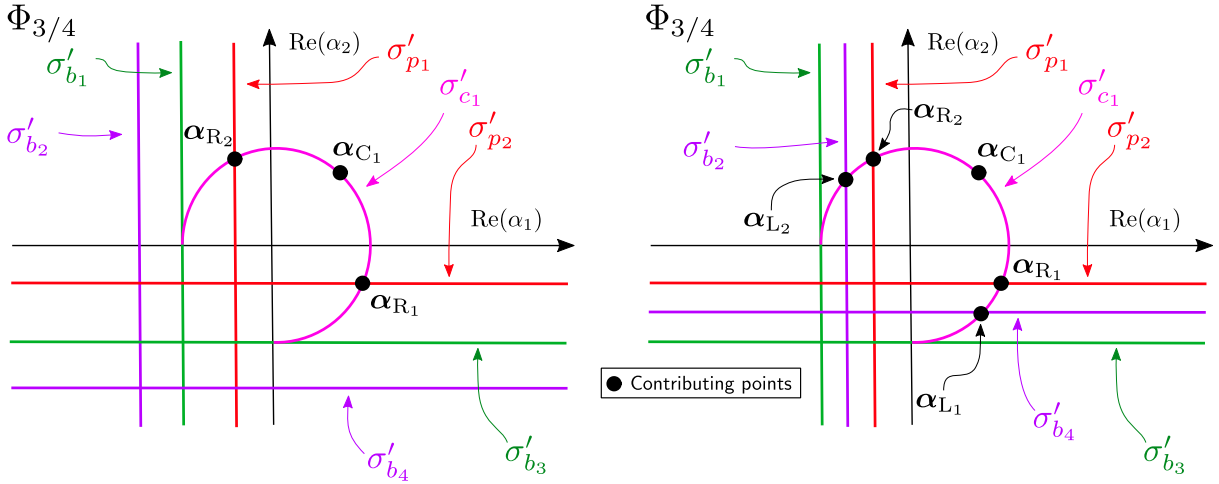


Figure 12: Contributing points of $\Phi_{3/4}$ for $k_1 < k_2$ (left) and $k_1 > k_2$ (right).

We often omit the detailed calculations in the following analysis, as they are similar to calculations shown previously. The details can be found in (Kunz, 2023), Chapter 5.

6.3.1 The reflected waves

The reflected waves ϕ_{R_1} and ϕ_{R_2} corresponding to the points α_{R_1} and α_{R_2} are obtained similarly to how the transmitted wave ψ_{T_1} was obtained in Section 6.2.1, so we omit the details (only the additive external term in (5.6) needs to be considered).

One then finds

$$\phi_{R_1}(\mathbf{x}) = \frac{\mathbf{a}_1 + \sqrt{k_2^2 - \mathbf{a}_2^2}}{\mathbf{a}_1 - \sqrt{k_2^2 - \mathbf{a}_2^2}} e^{-i(-\mathbf{a}_1 x_1 + \mathbf{a}_2 x_2)} \mathcal{H}(-x_1 \mathbf{a}_2 - x_2 \mathbf{a}_1) \mathcal{H}(-x_1). \quad (6.22)$$

and

$$\phi_{R_2}(\mathbf{x}) = \frac{\mathbf{a}_2 + \sqrt{k_2^2 - \mathbf{a}_1^2}}{\mathbf{a}_2 - \sqrt{k_2^2 - \mathbf{a}_1^2}} e^{-i(x_1 \mathbf{a}_1 - x_2 \mathbf{a}_2)} \mathcal{H}(-x_1 \mathbf{a}_2 - x_2 \mathbf{a}_1) \mathcal{H}(-x_2). \quad (6.23)$$

These formulae agree perfectly with the corresponding wave-fields predicted by GO (which are displayed in Fig. 4).

6.3.2 The cylindrical diffracted wave

Let us now study the contributing behaviour of Φ near $\alpha^* = \alpha_{C_1}(\vartheta) = -k_1 \tilde{\mathbf{x}}$. This is an isolated SOS on σ'_{c_1} with respect to $\tilde{\mathbf{x}}$. The bridge and arrow configuration is displayed in Fig. 9. Observing that Ψ_{++} is regular at $\alpha_{C_1}(\vartheta)$, the wave component ϕ_C corresponding to the SOS $\alpha_{C_1}(\vartheta)$ can be computed similarly to how the wave ψ_C was computed, so we omit the details. We find that

$$\phi_C(\mathbf{x}) = \frac{\Psi_{++}(k_1 \cos(\vartheta), k_1 \sin(\vartheta))}{8\sqrt{2\pi}} \left(1 - \frac{k_2^2}{k_1^2}\right) e^{-i3\pi/4} \times \frac{e^{-ik_1 r}}{\sqrt{k_1 r}}. \quad (6.24)$$

The quantity

$$D_{\phi_C}(\vartheta, \vartheta_0) = \frac{\Psi_{++}(k_1 \cos(\vartheta), k_1 \sin(\vartheta))}{8\sqrt{2\pi}} \left(1 - \frac{k_2^2}{k_1^2}\right) e^{-i3\pi/4}$$

corresponds to the (cylindrical) diffraction coefficient of ϕ_{sc} .

6.3.3 The lateral diffracted waves

If $k_1 < k_2$, the wave components of ϕ_{sc} are given by ϕ_{R_1} , ϕ_{R_2} , and ϕ_{C_1} . In this case, the wave components of ψ include the lateral waves ψ_{L_1} and ψ_{L_2} . However, when $k_1 > k_2$, these lateral waves are present on the wedges exterior and correspond to the crossings $\sigma'_{b_2} \cap \sigma'_{c_1}$ and $\sigma'_{b_4} \cap \sigma'_{c_1}$, respectively, as we will prove in this section. We label these crossings as α_{L_2} and α_{L_1} , respectively. This agrees with how we labelled the crossings of σ'_{b_3} and σ'_{b_1} with σ'_{c_2} , which led to the lateral waves on the wedge's interior. However, there is no ambiguity whether these points correspond to crossings of singularities of $\Phi_{3/4}$, or Ψ_{++} : whenever $k_1 < k_2$, these points correspond to crossings of singularities of Ψ_{++} and whenever $k_2 < k_1$, they correspond to crossings of singularities of $\Phi_{3/4}$. Thus, in either case, the points α_{L_1} and α_{L_2} correspond to the total wave-field's (only) two lateral waves. Let $k_1 > k_2$.

The lateral wave ϕ_{L_2} . Let us begin by studying the contributing behaviour of $\Phi_{3/4}$ near the point $\alpha^* = \alpha_{L_2}$. To this end, we study the contributing behaviour of $-K\Psi_{++} = -\Phi$. Since $\Phi_{3/4} = -\Phi - P_{++}$, and since P_{++} does not exhibit a crossing of singularities at α_{L_2} , the contributing behaviour of $-\Phi$ completely determines the contributing behaviour of $\Phi_{3/4}$. Let $\sigma_1 = \sigma_{c_1}$ and $\sigma_2 = \sigma_{b_2}$. Similarly to Section 6.2.3, we assume that $k_2 \neq \sqrt{2}k_1$.

Step 1. Choose $g_1(\alpha) = k_1^2 - \alpha_1^2 - \alpha_2^2$ and $g_2(\alpha) = \alpha_2 + k_2$. Since $\mathbf{e}_r = -\mathbf{n}_1^*$ and $\mathbf{e}_{\text{Re}(\alpha_1)} = \mathbf{n}_2^*$, and since the bridge and arrow configuration at α_{L_2} is as displayed in Fig. 9, we find that the sign factors are given by $s_1 = s_2 = +1$.

Step 2. For $\varkappa > 0$, we have $\alpha_{L_2} \in \text{LHP} \times \text{UHP}$. Let us use the formula (5.6) to study the contributing asymptotic behaviour of Φ . Then, just as in Section 6.2.3, we find that the contributing asymptotic behaviour of Φ is given by

$$-\Phi(\alpha) \underset{\sim}{\text{contr.}} -\frac{1}{2} \left(\frac{(k_2^2 - k_1^2) \Psi_{++} \left(\alpha_1, \sqrt[3]{k_1^2 - \alpha_1^2} \right)}{\left(\sqrt[3]{k_1^2 - \alpha_1^2} - \alpha_2 \right) \sqrt[3]{k_1^2 - \alpha_1^2}} \right), \text{ as } \alpha \rightarrow \alpha_{L_2}. \quad (6.25)$$

Now, for α_1 close to $-k_2$, we have

$$K_{o+} \left(\alpha_1, \sqrt[3]{k_1^2 - \alpha_1^2} \right) \Psi_{++} \left(\alpha_1, \sqrt[3]{k_1^2 - \alpha_1^2} \right) = \frac{-i}{4\pi} \int_P \mathcal{I}_2 \left(\alpha_1, \sqrt[3]{k_1^2 - \alpha_1^2}; z_2 \right) dz_2 \\ - \frac{K_{-o}(\alpha_1, \mathbf{a}_2) P_{++} \left(\alpha_1, \sqrt[3]{k_1^2 - \alpha_1^2} \right)}{K_{o+} \left(\alpha_1, \sqrt[3]{k_1^2 - \alpha_1^2} \right) K_{o-}(\alpha_1, \mathbf{a}_2) K_{-o}(\mathbf{a}_1, \mathbf{a}_2)}. \quad (6.26)$$

Contrary to how the lateral waves on the wedges interior were analysed, the integral term in (6.26) is non-regular at $\alpha_1 = -k_2$ (and so is the external additive term), so we cannot directly proceed as in Section 6.2.3.

Now, a lengthy but straightforward calculation shows that

$$K_{o+} \left(\alpha_1, \sqrt[3]{k_1^2 - \alpha_1^2} \right) \Psi_{++} \left(\alpha_1, \sqrt[3]{k_1^2 - \alpha_1^2} \right) = \\ \frac{-i}{4\pi} \int_P \left(\mathcal{I}_2 \left(\alpha_1, \sqrt[3]{k_1^2 - \alpha_1^2}; z_2 \right) - \mathcal{I}_2 \left(\alpha_1, -\sqrt[3]{k_2^2 - \alpha_1^2}; z_2 \right) \right) dz_2 + \frac{\Phi \left(\alpha_1, -\sqrt[3]{k_2^2 - \alpha_1^2} \right)}{K_{o-} \left(\alpha_1, -\sqrt[3]{k_2^2 - \alpha_1^2} \right)} \\ + \frac{P_{++} \left(\alpha_1, -\sqrt[3]{k_2^2 - \alpha_1^2} \right) - P_{++} \left(\alpha_1, \sqrt[3]{k_1^2 - \alpha_1^2} \right)}{K_{o-}(\alpha_1, \mathbf{a}_2)}. \quad (6.27)$$

The first and the third term on the right hand side of (6.27) can be shown to be regular as $\alpha_1 \rightarrow -k_2$. Therefore, using (6.25), we conclude that

$$\Phi(\alpha) \underset{\sim}{\text{contr.}} -\frac{1}{2} \frac{(k_2^2 - k_1^2)}{\left(\sqrt[3]{k_1^2 - \alpha_1^2} - \alpha_2 \right) \sqrt[3]{k_1^2 - \alpha_1^2}} \frac{1}{K_{o+} \left(\alpha_1, \sqrt[3]{k_1^2 - \alpha_1^2} \right)} \frac{\Phi \left(\alpha_1, -\sqrt[3]{k_2^2 - \alpha_1^2} \right)}{K_{o-} \left(\alpha_1, -\sqrt[3]{k_2^2 - \alpha_1^2} \right)},$$

as $\alpha \rightarrow \alpha_{L_2}$, and it can be shown, just as in Section 6.2.3, that the function $\Phi(\alpha_1, -\sqrt[3]{k_2^2 - \alpha_1^2})/K_{o-}(\alpha_1, -\sqrt[3]{k_2^2 - \alpha_1^2})$ is regular as $\alpha_1 \rightarrow -k_2$. We can thus define the quantity

$$\mathcal{L}_{\phi_{L_2}}(\vartheta_0) = \lim_{\alpha_1 \rightarrow -k_2} \frac{\Phi \left(\alpha_1, -\sqrt[3]{k_2^2 - \alpha_1^2} \right)}{K_{o-} \left(\alpha_1, -\sqrt[3]{k_2^2 - \alpha_1^2} \right)}. \quad (6.28)$$

Proceeding as in Section 6.2.3, we find that

$$\Phi(\alpha) \underset{\sim}{\text{contr.}} A \times g_1(\alpha)^{-m_1} \times g_2(\alpha)^{-m_2}, \text{ as } \alpha \rightarrow \alpha_{L_2}$$

with $m_1 = 1$, $m_2 = -1/2$ and

$$A = -2\sqrt{k_1^2 - k_2^2} \sqrt{2k_2} \mathcal{L}_{\phi_{L_2}}(\vartheta_0).$$

Step 3. We use (5.15) to compute the corresponding wave component ϕ_{L_1} . Introducing the lateral diffraction coefficient

$$D_{\phi_{L_2}}(\vartheta_0) = -\frac{2(k_1^2 - k_2^2)^{3/4} \sqrt{k_2} e^{i3\pi/4} \mathcal{L}_{\phi_{L_2}}(\vartheta_0)}{\sqrt{\pi}}$$

we find that

$$\phi_{L_2}(\mathbf{x}) = D_{\phi_{L_2}}(\vartheta_0) \frac{e^{i(k_2 x_1 - \sqrt{k_1^2 - k_2^2} x_2)}}{|x_1 \sqrt{k_1^2 - k_2^2} + x_2 k_2|^{3/2}} \mathcal{H}\left(\sqrt{k_1^2 - k_2^2} x_1 + k_2 x_2\right) \mathcal{H}(-x_2). \quad (6.29)$$

The lateral wave ϕ_{L_1} . It remains to study the contributing asymptotic behaviour of Φ near α_{L_1} . This is done similarly to how the contributing asymptotics near α_{L_2} have been found, so we omit the details. Again, we can define the quantity

$$\mathcal{L}_{\phi_{L_1}}(\vartheta_0) = \lim_{\alpha_2 \rightarrow -k_2} \frac{\Phi\left(-\sqrt{k_2^2 - \alpha_2}, \alpha_2\right)}{K_{-\circ}\left(-\sqrt{k_2^2 - \alpha_2}, \alpha_2\right)},$$

and upon introducing the lateral diffraction coefficient

$$D_{\phi_{L_1}}(\vartheta_0) = -\frac{2(k_1^2 - k_2^2)^{3/4} \sqrt{k_2} e^{i3\pi/4} \mathcal{L}_{\phi_{L_1}}(\vartheta_0)}{\sqrt{\pi}}, \quad (6.30)$$

we find that

$$\phi_{L_1} = D_{\phi_{L_1}}(\vartheta_0) \frac{e^{i(-\sqrt{k_1^2 - k_2^2} x_1 + k_2 x_2)}}{|x_1 k_2 + x_2 \sqrt{k_1^2 - k_2^2}|^{3/2}} \mathcal{H}\left(k_1 x_1 + \sqrt{k_1^2 - k_2^2} x_2\right) \mathcal{H}(x_2). \quad (6.31)$$

As in Section 6.2.3, formulae (6.29) and (6.31) are in perfect agreement with the form of lateral waves we expect from the studies outlined in Section 4.1. When $k_1 < k_2$, we set $\phi_{L_1} = \phi_{L_2} \equiv 0$.

We have thus proved the correctness of (4.1) in the simple case, where the fields' GO components which are illustrated in Fig. 4 (left) are given by $\psi_{\text{GO}} = \psi_{T_1} + \psi_{T_2}$ and $\phi_{\text{GO}} = \phi_{\text{in}} + \phi_{R_1} + \phi_{R_2}$. The diffracted far-field, consisting of cylindrical and lateral diffracted waves, is described by equations (6.9), (6.19), (6.21), (6.24), (6.29), and (6.31), and is illustrated in Fig. 13.

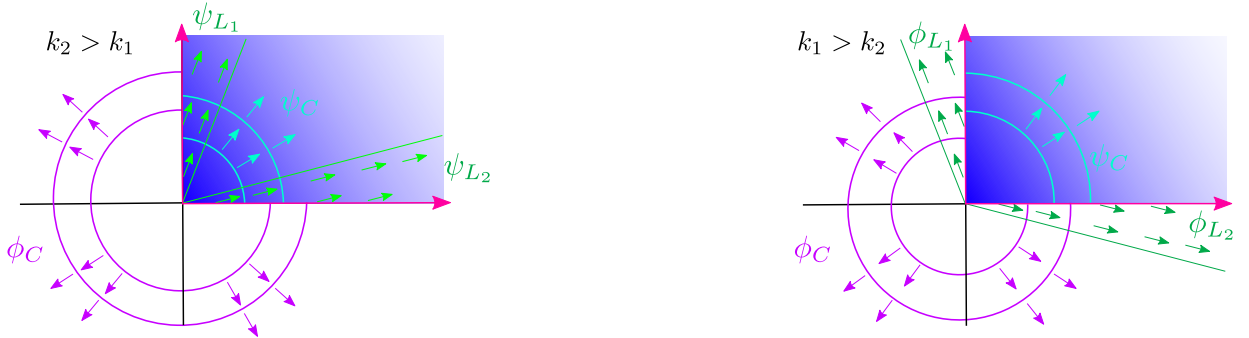


Figure 13: Diffracted wave components.

7 The complicated case

Let us now consider the case $\vartheta_0 \in (\pi/2, \pi)$. Note that in this case, we cannot directly impose the Sommerfeld radiation condition via the limiting absorption principle, although, of course, a radiation condition needs to be imposed. The failure of defining this via the absorption principle is due to the fact that for positive imaginary part $\varkappa > 0$ of k_1 and k_2 , such incident angle changes the sign of \mathbf{a}_2 : whereas in the simple case discussed in Section 6 we are guaranteed $\text{Im}(\mathbf{a}_1), \text{Im}(\mathbf{a}_2) < 0$ whenever $\varkappa > 0$ we now have $\text{Im}(\mathbf{a}_1) < 0$, and $\text{Im}(\mathbf{a}_2) > 0$ whenever $\varkappa > 0$. We circumvent this issue by working directly in Fourier space. That is, we treat ϑ_0 as an analytic parameter within the formulae for analytic continuation of Ψ_{++} and thus obtain formulae for Ψ_{++} when $\vartheta_0 \in (\pi/2, \pi)$. Here, by ‘analytic parameter’ we mean that the spectral functions depend analytically on ϑ_0 . The radiation condition is then formulated by imposing the *continuity of bypass*. If the arrow points to a given side of σ'_j in the simple case, then it must point to this side of σ'_j in the complicated case. By uniqueness of analytic continuation and Stokes’ theorem, this condition uniquely determines ψ and ϕ_{sc} in the complicated case. Defining the physical fields in this way *seems* to be a sensible way to impose the radiation condition for the following reasons.

1. It leads to the GO components one would expect for the complicated case, as we will prove during this Section.
2. It prohibits the existence of any unphysical wave-fields.
3. It implies that the physical fields depend continuously on the incident angle.

However, note that the analytic dependence of Ψ_{++} on ϑ_0 , of which the preceding points are a consequence, is, at this point, only an assumption. For a more detailed discussion involving the intricacies of formulating the radiation condition in the complicated case, we refer to (Assier et al., 2023), Section 2.

As mentioned in (Kunz and Assier, 2023), in the complicated case we also obtain new singularities within the formulae for analytic continuation. Namely, the external additive term in (5.5) becomes singular at

$$\sigma_{sp} = \left\{ \boldsymbol{\alpha} \in \mathbb{C}^2 \mid \boldsymbol{\alpha}_1 \equiv -\sqrt[3]{k_2^2 - \mathbf{a}_2^2} \right\},$$

which, for $\vartheta_0 \in (\pi/2, \pi)$, is a polar singularity. Here, the subscript $_{sp}$ stands for ‘secondary pole’, since, as we shall see, it will lead to the existence of secondary reflected and transmitted waves. Note that for $\vartheta_0 = \pi$, we have $\sigma_{sp} = \sigma_{b_2}$. Therefore, imposing the aforementioned continuity of bypass, we find that the bridge and arrow configuration on σ_{sp} is as displayed in Fig. 14. Moreover, the singularity σ_{p_2} changes half-plane during such change of incident angle since the parameter \mathbf{a}_2 changes its sign (as is displayed in Fig. 14). Note that formulae (5.5) and (5.6) remain valid in the complicated case.

The singularities for the complicated case and the corresponding bridge and arrow configurations are displayed in Fig. 14. We now discuss how this change of singularity structure affects the physical far-field.

The diffracted waves. The cylindrical and lateral diffracted waves are computed exactly as in the simple case, since the points $\boldsymbol{\alpha}_{C_1}, \boldsymbol{\alpha}_{C_2}, \boldsymbol{\alpha}_{L_1}$, and $\boldsymbol{\alpha}_{L_2}$ whose contributions yield these waves are unaffected by the change of incident angle. That is, formulae (6.9) (for ψ_C), (6.24) (for ϕ_C), (6.19) (for ψ_{L_2}), (6.21) (for ψ_{L_1}), (6.29) (for ϕ_{L_2}), and (6.31) (for ϕ_{L_1}) remain valid in the complicated case.

Non-contributing points. Similar to how the non-contributing points in the simple case were analysed in Section 6.1, it can be shown that the points highlighted in Fig. 14 are non-

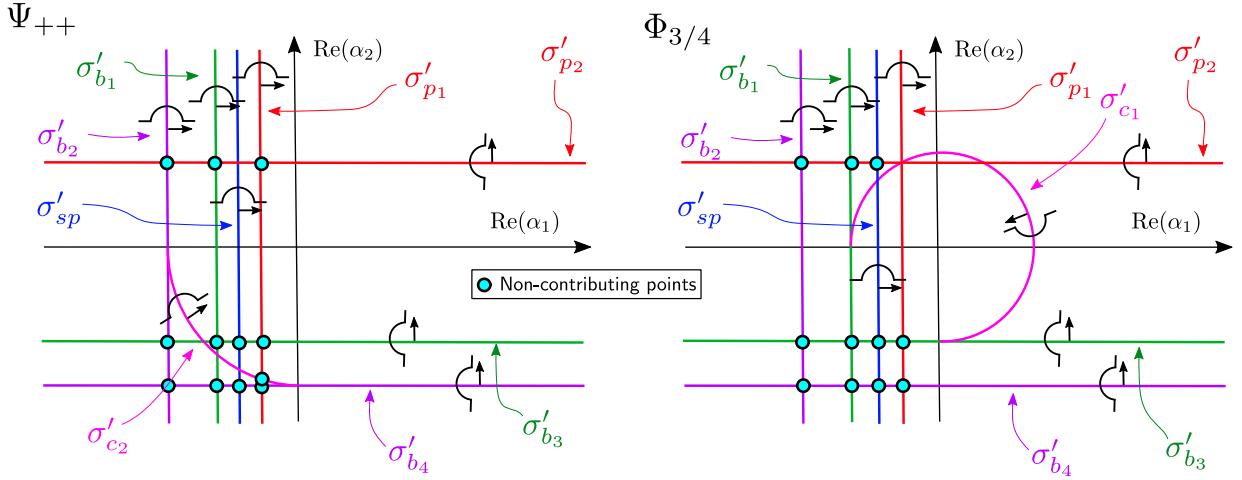


Figure 14: Real traces of the spectral functions' irreducible singularities, corresponding bridge and arrow configuration, and non-contributing points.

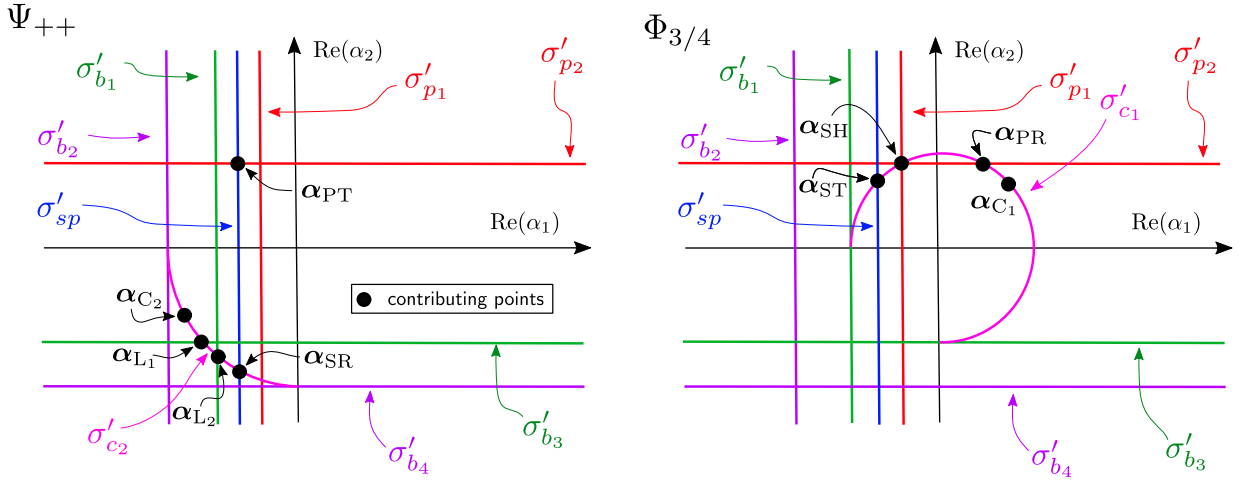


Figure 15: Contributing points in the complicated case.

contributing.

To obtain the wave components of ψ and ϕ , it thus remains to consider the contributing behaviour of Ψ_{++} at the points

$$\alpha_{\text{PT}} = \left(-\sqrt[3]{k_2^2 - a_2^2}, a_2 \right), \quad \alpha_{\text{SR}} = \left(-\sqrt[3]{k_2^2 - a_2^2}, -a_2 \right),$$

and the contributing behaviour of $\Phi_{3/4}$ at the points

$$\alpha_{\text{PR}} = (-a_1, a_2), \quad \alpha_{\text{SH}} = (a_1, a_2), \quad \alpha_{\text{ST}} = \left(-\sqrt[3]{k_2^2 - a_2^2}, \sqrt[3]{k_1^2 - k_2^2 + a_2^2} \right).$$

Here, as in Section 4, the subscripts PT, SR, PR, and ST stand for 'primary transmitted', 'secondary reflected', 'primary reflected', and 'secondary transmitted', respectively. The subscript SH corresponds to 'shadow', as this crossing will yield the expected shadow region.

The contributing points, including those which yield the diffracted waves, are, for $k_2 > k_1$, displayed in Fig. 15. Since all of the following computations are analogous to those done in the simple case, we will be brief.

7.1 Geometrical optics components of ψ and ϕ

The computations yielding the wave-field's GO components in the complicated case are similar to those which yielded the transmitted wave ψ_{T_1} : The corresponding wave component can always be computed by solely studying the additive term in either (5.5) or (5.6), respectively. We thus only give the results, and refer to (Kunz, 2023) for the computational details. As before, in the following discussion, the waves' subscripts correspond to the points from which they are obtained.

GO components of ψ . Let us assume that $k_2^2 - \mathbf{a}_2^2 > 0$. This is always the case if $k_2 > k_1$, but when $k_1 > k_2$, we may have $k_2^2 - \mathbf{a}_2^2 < 0$. If that is the case, we have $\sigma'_{sp} = \emptyset$ and obtain no corresponding wave components. Indeed, the case of $k_2^2 - \mathbf{a}_2^2 < 0$ corresponds to total internal reflection on the wedges exterior.

We then find

$$\psi_{PT}(\mathbf{x}) = \frac{2\mathbf{a}_1}{\mathbf{a}_1 - \sqrt{k_2^2 - \mathbf{a}_2^2}} e^{-i(\sqrt{k_2^2 - \mathbf{a}_2^2}x_1 + \mathbf{a}_2x_2)} \mathcal{H}(x_1)\mathcal{H}(x_2), \quad (7.1)$$

and

$$\psi_{SR}(\mathbf{x}) = \frac{\mathbf{a}_2 - \sqrt{k_1^2 - k_2^2 + \mathbf{a}_2^2}}{\mathbf{a}_2 + \sqrt{k_1^2 - k_2^2 + \mathbf{a}_2^2}} \frac{2\mathbf{a}_1 e^{i(\sqrt{k_2^2 - \mathbf{a}_2^2}x_1 + \mathbf{a}_2x_2)}}{\mathbf{a}_1 - \sqrt{k_2^2 - \mathbf{a}_2^2}} \mathcal{H}\left(\mathbf{a}_2x_1 - \sqrt{k_2^2 - \mathbf{a}_2^2}x_2\right) \mathcal{H}(x_2). \quad (7.2)$$

Both, ψ_{PT} and ψ_{SR} agree with the corresponding GO components, which are illustrated in Fig. 4, right.

GO components of ϕ . Let us now moreover assume that $k_1^2 > k_2^2 - \mathbf{a}_2^2 \geq 0$. If $k_1^2 = k_2^2 - \mathbf{a}_2^2$, we get no contribution from the point α_{ST} since the crossing becomes tangential. If $k_1^2 < k_2^2 - \mathbf{a}_2^2$, we get no contribution since the singularity σ_{sp} does not cross the circle σ_{c_1} . We will see that as k_1 approaches $\sqrt{k_2^2 - \mathbf{a}_2^2}$, the secondary transmitted wave vanishes. The case $k_1 \leq \sqrt{k_2^2 - \mathbf{a}_2^2}$ thus corresponds to total internal reflection of the primary transmitted wave within the wedges interior. Overall, we then have

$$\phi_{ST}(\mathbf{x}) = \frac{4\mathbf{a}_1\mathbf{a}_2 \times e^{i(\sqrt{k_2^2 - \mathbf{a}_2^2}x_1 - \sqrt{k_1^2 - k_2^2 + \mathbf{a}_2^2}x_2)}}{(\mathbf{a}_1 - \sqrt{k_2^2 - \mathbf{a}_2^2})(\mathbf{a}_2 + \sqrt{k_1^2 - k_2^2 + \mathbf{a}_2^2})} \mathcal{H}\left(x_1\sqrt{k_1^2 - k_2^2 + \mathbf{a}_2^2} + x_2\sqrt{k_2^2 - \mathbf{a}_2^2}\right) \mathcal{H}(-x_2), \quad (7.3)$$

$$\phi_{PR}(\mathbf{x}) = \frac{\mathbf{a}_1 + \sqrt{k_2^2 - \mathbf{a}_2^2}}{\mathbf{a}_1 - \sqrt{k_2^2 - \mathbf{a}_2^2}} e^{-i(-\mathbf{a}_1x_1 + \mathbf{a}_2x_2)} \mathcal{H}(-x_1\mathbf{a}_2 - x_2\mathbf{a}_1)\mathcal{H}(-x_1), \quad (7.4)$$

and

$$\phi_{SH}(\mathbf{x}) = -e^{-i(\mathbf{a}_1x_1 + \mathbf{a}_2x_2)} \mathcal{H}(-x_2)\mathcal{H}(x_1\mathbf{a}_2 - x_2\mathbf{a}_1). \quad (7.5)$$

Note that ϕ_{SH} annihilates the incident wave ϕ_{in} within the region $\{x_1\mathbf{a}_2 - x_2\mathbf{a}_1 > 0, x_2 < 0\}$, which leads to the expected shadow region. The formulae that are given above yield the anticipated GO wave components, which are illustrated in Fig. 4, right.

Remark 7.1. The points α_{SH} yields a triple crossing of singularities. To apply the framework developed in (Assier et al., 2022), it thus needs to be reduced to a double crossing, which can be done by computing the contributing behaviour of $\Phi_{3/4}$ near α_{SH} (see (Kunz, 2023)). However, in general, not every triple crossing is reducible to a double crossing, and in fact, such crossings do occur in the quarter-plane problem (Assier et al., 2023), Section 4.

We have thus proved the correctness of (4.1) in both, the simple and the complicated case. In the complicated case, the fields' GO components, which are illustrated in Fig. 4 (right), are given by $\psi_{GO} = \psi_{PT} + \psi_{SR}$ and $\phi_{GO} = \phi_{in} + \phi_{PR} + \phi_{ST} + \phi_{SH}$, and the diffracted far-field is as in the simple case.

8 Concluding remarks

In this article, we have used the machinery developed in (Assier et al., 2022) to prove the correctness of equation (4.1), and thus gave a closed-form description of the far-field encountered in the right-angled no-contrast penetrable wedge diffraction problem. Although the corresponding cylindrical and lateral diffraction coefficients remain unknown, we found that they can be expressed in terms of the spectral functions Ψ_{++} and Φ as described in Sections 6.3.2 (for ψ_C), 6.2.3 (for ψ_{L_1} and ψ_{L_2}), 6.3.2 (for ϕ_C) and 6.3.3 (for ϕ_{L_1} and ϕ_{L_2}). Moreover, we have shown that by imposing Sommerfeld’s radiation condition via the limiting absorption principle and continuity of bypass on the scattered fields (as opposed to the diffracted fields), we recover the GO components which are predicted by Snell’s law and the law of reflection.

We plan on using the system of integral equations presented in Theorem 4.2.1 of (Kunz and Assier, 2022) to construct rational approximations of Ψ_{++} and Φ , akin to the scheme that was proposed by Assier and Abrahams (2020). It is hoped that such approximations will allow for rapid and accurate computation of the diffraction coefficients.

The wave components we have derived are invalid on the GO lines of discontinuity and on the wedges interface. Describing the waves within these regions requires the study of non-isolated saddles on singularities. Developing a framework that allows for this, and obtaining a uniform far-field approximation, will be the focus of future work.

Acknowledgements

Valentin D. Kunz would like to acknowledge funding by the University of Manchester (Dean’s scholarship award).

References

- Assier, R. C. and Abrahams, I. D. (2020). On the asymptotic properties of a canonical diffraction integral. *Proc. R. Soc. A Math. Phys. Eng. Sci.*, 476:20200150.
- Assier, R. C. and Abrahams, I. D. (2021). A surprising observation on the quarter-plane diffraction problem. *SIAM J. Appl. Math.*, 81(1):60–90.
- Assier, R. C. and Shanin, A. V. (2019). Diffraction by a quarter-plane. Analytical continuation of spectral functions. *Q. J. Mech. Appl. Math.*, 72(1):51–86.
- Assier, R. C. and Shanin, A. V. (2021a). Analytical continuation of two-dimensional wave fields. *Proc. R. Soc. A Math. Phys. Eng. Sci.*, 477(20200681).
- Assier, R. C. and Shanin, A. V. (2021b). Vertex Green’s functions of a quarter-plane. links between the functional equation, additive crossing and Lamé functions. *Q. J. Mech. Appl. Math.*, 74(3):251–295.
- Assier, R. C., Shanin, A. V., and Korolkov, A. I. (2022). A contribution to the mathematical theory of diffraction: a note on double Fourier integrals. *Q. J. Mech. Appl. Math.*, 76(1):1–47.
- Assier, R. C., Shanin, A. V., and Korolkov, A. I. (2023). A contribution to the mathematical theory of diffraction. Part II: Recovering the far-field asymptotics of the quarter-plane problem. *Submitted to Q. J. Mech. Appl. Math.; arXiv:2310.18031*.
- Babich, V. M. and Mokeeva, N. V. (2008). Scattering of the plane wave by a transparent wedge. *J. Math. Sci.*, 155(3):335–342.

- Borovikov, V. A. and Kinber, B. Y. (1993). *Geometrical theory of diffraction*. IEE Electromagnetic Waves Series 37, London.
- Brekhovskikh, L. and Godin, O. (1999). *Acoustics of layered media II, 2nd edition*, volume 10 of *Wave phenomena*. Springer, Berlin, Heidelberg.
- Chirka, E. M. (1989). *Complex Analytic Sets*. Mathematics and its Applications. Springer, Dordrecht.
- Keller, J. B. (1962). Geometrical theory of diffraction. *Journal of the Optical Society of America*, 52:116–130.
- Kraut, E. A. and Lehmann, G. W. (1969). Diffraction of electromagnetic waves by a right-angle dielectric wedge. *Journal of Mathematical Physics*, 10:1340–1348.
- Kunz, V. D. (2023). A two-complex-variable approach to wave diffraction by a no-contrast penetrable wedge; PhD Thesis. *Submitted for examination*.
- Kunz, V. D. and Assier, R. C. (2022). Diffraction by a Right-Angled No-Contrast Penetrable Wedge Revisited: A Double Wiener-Hopf Approach. *SIAM J. Appl. Math.*, 82(4):1495–1519.
- Kunz, V. D. and Assier, R. C. (2023). Diffraction by a Right-Angled No-Contrast Penetrable Wedge: Analytical Continuation of Spectral Functions. *Q. J. Mech. Appl. Math.*, hbad002.
- Lawrie, J. B. and Abrahams, I. D. (2007). A brief historical perspective of the Wiener-Hopf technique. *J. Eng. Math.*, 59:351–358.
- Madsen, I. H. and Tornehave, J. (1997). *From Calculus to Cohomology: De Rham Cohomology and Characteristic Classes*. Mathematics and its Applications. Cambridge University Press.
- Nethercote, M. A. (2019). Effective analytic and asymptotic procedures for wave diffraction by perfect and penetrable wedges; PhD Thesis. *The University of Manchester*.
- Nethercote, M. A., Assier, R. C., and Abrahams, I. D. (2020). High-contrast approximation for penetrable wedge diffraction. *IMA J. Appl. Math.*, 85(3):421–466.
- Noble, B. (1958). *Methods Based on the Wiener-Hopf Technique*. Pergamon Press London, New York, Paris, Los Angeles.
- Radlow, J. (1964). Diffraction by a right-angled dielectric wedge. *Int. J. Eng. Sci.*, 2:275–290.
- Shabat, B. V. (1991). *Introduction to Complex Analysis Part II Functions of Several Variables*. American Mathematical Society, Providence, Rhode Island.
- Stoker, J. J. (1956). On radiation conditions. *Comm. Pure Appl. Math.*, IX:577–596.